The δ-ALE-SPH model: an arbitrary Lagrangian-Eulerian framework for the δ-SPH model with Particle Shifting Technique

M. Antuono [a], P. N. Sun [b,c], S. Marrone [a], A.-M. Zhang [d], A. Colagrossi [a,c,*],

[a] *CNR-INM, INstitute of Marine engineering, Rome, Italy*

[b] *School of Marine Engineering and Technology, Sun Yat-sen University, Zhuhai, 519000, China*

[c] *Ecole Centrale Nantes, LHEEA res. dept. (ECN and CNRS), Nantes, France*

[d] *College of Shipbuilding Engineering, Harbin Engineering University, Harbin, China*

Abstract

In the present work we study the behaviour of a weakly-compressible SPH scheme obtained by rewriting the Navier-Stokes equations in an arbitrary Lagrangian-Eulerian (ALE) format. Conversely to previous theoretical works the proposed SPH model is expressed in terms of primitive variables (i.e. density and velocity) instead of conservative ones. Differently from the classical approach to ALE, which is based on the use of Riemann solvers inside the spatial operators , the present model is written by using the standard differential formulations of the weakly-compressible SPH schemes. As other ALE-SPH models, the arbitrary velocity field is obtained by modifying the pure Lagrangian velocity of the material point through a velocity $\delta \boldsymbol{u}$ given by a Particle Shifting Technique (PST). We show that the above-mentioned ALE-SPH equations are, however, unstable when they are integrated in time. The instability appears in the form of large volume variations in those fluid regions characterised by high velocity strain rates. Nonetheless, the scheme can be stabilised if appropriate diffusion terms are included in both the equations of density and mass. This latter scheme, hereinafter called δ-ALE-SPH scheme, is validated against reference benchmark test-cases: the viscous flow around an inclined elliptical cylinder, the lid-driven cavity and a dam-break flow impacting a vertical wall.

Key words: Delta-SPH, Smoothed Particle Hydrodynamics, Arbitrary-Lagrangian-Eulerian, SPH accuracy, Particle shifting, SPH consistency.

1 Introduction

The Smoothed Particle Hydrodynamics (SPH) is a meshless particle method, initially conceived in the context of astrophysics and subsequently applied to different fields of physics (as, for example, fluid dynamics and solid mechanics). Over the years, several variants of the original Lagrangian scheme have been proposed. Among these, the δ-SPH has proved to be a robust and reliable method in solving several hydrodynamic problems, (see *e.g.* [1, 2, 6, 7, 21, 22, 30, 35, 36, 37]). Nevertheless, there are still some drawbacks that limit its application in some areas where traditional CFD methods perform well, such as the modelling of shear flows at high Reynolds numbers, vortical flow evolutions characterized by large negative pressure values or viscous flows inside confined domains.

To solve these problems, Sun et al. [28] combined the Particle Shifting Technique (PST) within the δ-SPH scheme, obtaining the δ^+-SPH scheme. It was shown that the use of the PST allows to get regular particle spatial distribution, a condition necessary to reduce errors in the SPH differential operators and to guarantee a convergence order larger than unity (see *e.g.* [5]). It was also shown that PST helps obtaining a smoother velocity distribution and, consequently, improves the field of vorticity. Unfortunately, despite these strong points, δ^+-SPH still presents some drawbacks, especially when body forces are present. In these circumstances the shifting velocity yields non-physical changes on the potential energy of the particles which can accumulate

* Corresponding author: *Tel.: +39 06 50 299 343; Fax: +39 06 50 70 619.*
Email address: andrea.colagrossi@cnr.it (A. Colagrossi).

errors in time. Recently, Sun et al. [29] proposed a different derivation of the δ^+-SPH that allows for a convincing inclusion of PST in the δ-SPH scheme and, at the same time, overcomes the above-mentioned issues.

The present work is dedicated to a further extension of the δ^+-SPH scheme within the framework of the Arbitrary Lagrangian Eulerian (ALE) formulation recently proposed in Oger et al. [24]. Thanks to the latter approach, the shifting velocity can be added in a consistent way and the overall scheme can be regarded as a generalization of that derived in Sun et al. [29]. In fact, the δ^+-SPH scheme of [29] can be obtained back as a simplified version of the proposed model. This, hereinafter denoted δ-ALE-SPH, shares some similarities with the ALE scheme described in Oger et al. [24]. The main difference is that, in the latter scheme, Riemann solvers are used for the particle mass and momentum exchanges and are responsible for the generation of an implicit numerical diffusion. On the contrary, in the δ-ALE-SPH the numerical diffusion terms are added explicitly and can be controlled straightforwardly. In particular, the diffusion is added both in the continuity equation (written in terms of the density field) and in the equation for the particle mass. We show that both the above models, namely the ALE and the δ-ALE-SPH schemes, are unstable if the diffusive terms (implicit or explicit) are not included.

In the δ-ALE-SPH the shifting velocity introduces changes for both volumes and masses of the particles. However, thanks to the PST structure, the relative variations of the particle volumes and masses are limited to few percent. Furthermore, those variations decrease with the particle's size, since the magnitude of the shifting velocity term decreases accordingly.

Differently from the standard ALE approach (see, for example, [24]), we show that the δ-ALE-SPH can be derived by rearranging the Lagrangian time derivatives in the Navier-Stokes equation through the actual velocity field (that is, fluid velocity plus shifted velocity) and by adding the Reynolds Transport Theorem to the derived set of equations. In particular, the latter equation is required to ensure a consistent modelling of the time evolution of elementary masses and volumes.

Then, the conservation properties of the δ-ALE-SPH are described and discussed in detail. Furthermore, two simplified variants of the proposed δ-ALE-SPH model are derived, showing, at least heuristically, only minor differences in the results among them.

2 The Navier-Stokes Equations for weakly-compressible flows in an ALE framework

In the present section we consider the Navier-Stokes (N.S.) equations for a weakly-compressible, barotropic fluid. We first consider a pure Lagrangian framework and, successively, we introduce an arbitrary transport velocity and rewrite the equation in an Arbitrary Lagrangian-Eulerian (ALE) framework.

The N.S. equations for a weakly-compressible fluid in a Lagrangian framework read as:

$$\begin{cases} \dfrac{\mathrm{D}\rho}{\mathrm{D}t} = -\rho\,\mathrm{div}(\boldsymbol{u})\,, \\ \dfrac{\mathrm{D}\boldsymbol{u}}{\mathrm{D}t} = -\dfrac{\nabla p}{\rho} + \dfrac{\mathrm{div}\,\mathbb{V}}{\rho} + \boldsymbol{g}\,, \\ \dfrac{\mathrm{D}\boldsymbol{r}}{\mathrm{D}t} = \boldsymbol{u}\,, \qquad p = c_0^2\,(\rho - \rho_0)\,. \end{cases} \tag{1}$$

where $\rho\,, \boldsymbol{u}$ are the primitive variables, namely the density and the velocity, $\boldsymbol{g}$ represents a generic volume force, while $\mathbb{V}$ is the viscous stress tensor. The pressure p is linked to the density field with a simple linear state equation where the density ρ_0 is the density at rest condition. In order to limit the variations of the density below 1%, the speed of sound c_0 needs to be chosen suitably (for more details see *e.g.* [23]). The last equation of (1) describes the trajectory of a generic material point at the position $\boldsymbol{r}$.

The derivative Df/Dt is the Lagrangian derivative of a generic fluid variable f, namely:

$$\frac{\mathrm{D}f}{\mathrm{D}t} := \frac{\partial f}{\partial t} + \nabla f \cdot \boldsymbol{u} \tag{2}$$

The ratio between the infinitesimal mass, m, and volume, V, of the material point $\boldsymbol{r}$ is finite and equal, by definition, to the density field $\rho = m/V$. In particular, the mass of the material point is conserved along the Lagrangian trajectory, i.e. $Dm/Dt = 0$. Combining the above relations with the continuity

equation in (1), we obtain the *Volumetric Strain Rate equation* (see *e.g.* [17]):

$$\frac{\mathrm{D}m}{\mathrm{D}t} = \frac{\mathrm{D}(\rho V)}{\mathrm{D}t} = 0 \qquad \Rightarrow \qquad \frac{\mathrm{D}V}{\mathrm{D}t} = V \mathrm{div}(\boldsymbol{u}) \,. \tag{3}$$

2.2 Navier-Stokes equations using a modified advection velocity $(\boldsymbol{u} + \delta\boldsymbol{u})$

We introduce now an arbitrary velocity deviation $\delta\boldsymbol{u}$ and define a second Lagrangian derivative with respect to the modified advection velocity $(\boldsymbol{u} + \delta\boldsymbol{u})$:

$$\frac{\mathrm{d}f}{\mathrm{d}t} := \frac{\partial f}{\partial t} + \nabla f \cdot (\boldsymbol{u} + \delta\boldsymbol{u}) = \frac{\mathrm{D}f}{\mathrm{D}t} + \nabla f \cdot \delta\boldsymbol{u} \,. \tag{4}$$

The last term on the right-hand side can be rewritten for generic scalar, f, and vector, $\boldsymbol{v}$, functions as follows:

$$\begin{cases} \nabla f \cdot \delta\boldsymbol{u} = \mathrm{div}(f\,\delta\boldsymbol{u}) - f\,\mathrm{div}(\delta\boldsymbol{u}) \,, \\ \nabla \boldsymbol{v} \cdot \delta\boldsymbol{u} = \mathrm{div}(\boldsymbol{v} \otimes \delta\boldsymbol{u}) - \boldsymbol{v}\,\mathrm{div}(\delta\boldsymbol{u}) \,. \end{cases} \tag{5}$$

Using the above notation, we can rewrite the Navier-Stokes equations using the modified time derivatives d/dt with the advection velocity $(\boldsymbol{u} + \delta\boldsymbol{u})$:

$$\begin{cases} \dfrac{\mathrm{d}\rho}{\mathrm{d}t} = -\rho\,\mathrm{div}(\boldsymbol{u} + \delta\boldsymbol{u}) + \mathrm{div}(\rho\,\delta\boldsymbol{u}) \,, \\ \dfrac{\mathrm{d}\boldsymbol{u}}{\mathrm{d}t} = -\dfrac{\nabla p}{\rho} + \dfrac{\mathrm{div}\,\mathbb{V}}{\rho} + \boldsymbol{g} + \mathrm{div}(\boldsymbol{u} \otimes \delta\boldsymbol{u}) - \boldsymbol{u}\,\mathrm{div}(\delta\boldsymbol{u}) \,, \\ \dfrac{\mathrm{d}\boldsymbol{r}}{\mathrm{d}t} = \boldsymbol{u} + \delta\boldsymbol{u} \,, \qquad p = c_0^2\,(\rho - \rho_0) \,. \end{cases} \tag{6}$$

The equation (6) becomes purely Lagrangian if $\delta\boldsymbol{u}$ is null (i.e. $df/dt = Df/Dt$), or pure Eulerian is $\delta\boldsymbol{u} = -\boldsymbol{u}$ (i.e. $df/dt = \partial f/\partial t$). Incidentally, we note that system (6) corresponds to the one adopted for the derivation of the consistent δ^+-SPH described in Sun et al. [29].

2.3 Navier-Stokes equations in an ALE formulation

To obtain the ALE formulation for the Navier-Stokes equations, we need to rewrite the relations for V through the time derivative d/dt. In any case, differently from the approach shown in the previous section, it is not possible to apply the formula (4) to the equations (3) straightforwardly. Indeed, in the ALE framework the volumes move with the modified velocity $\boldsymbol{u} + \delta\boldsymbol{u}$ and, consequently, the evolution equation is derived by using the Leibniz–Reynolds transport theorem. In particular, this leads to the following integral expressions:

$$\frac{\mathrm{d}V}{\mathrm{d}t} = \int_{S(t)} (\boldsymbol{u} + \delta\boldsymbol{u}) \cdot \boldsymbol{n}\, dS\,. \tag{7}$$

Using the divergence theorem on the surface integral and collapsing the finite volume $V(t)$ to an infinitesimal volume, we obtain

$$\frac{\mathrm{d}V}{\mathrm{d}t} = V \mathrm{div}(\boldsymbol{u} + \delta\boldsymbol{u})\,. \tag{8}$$

When $\delta\boldsymbol{u} = 0$, the above relation turns into Eq. (3). Conversely, for $\delta\boldsymbol{u} = -\boldsymbol{u}$, in the Eulerian framework the elementary portions of fluid will remain fixed in space (i.e. $d\boldsymbol{r}/dt = 0$) with a given fixed volume *i.e.* $\partial V/\partial t = 0$.

Finally, the equation (8) is included in the system (6) maintaining the usual

algebraic relation between mass, volume and density (namely $m = \rho V$). By rewriting the whole system in conservative variables (namely volume, mass and linear momentum), we obtain back the scheme described in Oger et al. [24], that is:

$$\begin{cases} \dfrac{\mathrm{d}V}{\mathrm{d}t} &= V \operatorname{div}(\boldsymbol{u} + \delta\boldsymbol{u}) \,, \\ \dfrac{\mathrm{d}m}{\mathrm{d}t} &= V \operatorname{div}(\rho\, \delta\boldsymbol{u}) \,, \\ \dfrac{\mathrm{d}(m\boldsymbol{u})}{\mathrm{d}t} &= -V \nabla p + V \operatorname{div} \mathbb{V} + m\, \boldsymbol{g} + V \operatorname{div}(\rho\, \boldsymbol{u} \otimes \delta\boldsymbol{u}) \,, \\ \dfrac{\mathrm{d}\boldsymbol{r}}{\mathrm{d}t} &= \boldsymbol{u} + \delta\boldsymbol{u} \,, \quad \rho = m \Big/ V \,, \quad p = c_0^2 \,(\rho - \rho_0) \,. \end{cases} \tag{9}$$

In [24] the above set of equation was derived by using a Leibniz-Reynolds transport theorem applied to an elementary portion of fluid moving with an arbitrary velocity $\boldsymbol{u}_0$, which in the present work corresponds to the velocity $(\boldsymbol{u} + \delta\boldsymbol{u})$. Finally, a Riemann SPH scheme was selected to model the particle interaction of the discrete system.

On the contrary, in the present work we model the spatial differential operators following the standard SPH framework and use a diffusive approach in analogy to the δ-SPH scheme. Specifically, the system (6) is rewritten in terms of mass and density and numerical diffusive terms are added in both the continuity

and mass equations, as follows:

$$\begin{cases} \dfrac{\mathrm{d}\rho}{\mathrm{d}t} &= -\rho\,\mathrm{div}(\boldsymbol{u}+\delta\boldsymbol{u}) + \mathrm{div}(\rho\,\delta\boldsymbol{u}) + \mathcal{D}^{\rho}\,, \\ \dfrac{\mathrm{d}m}{\mathrm{d}t} &= m\,\dfrac{\mathrm{div}(\rho\,\delta\boldsymbol{u})}{\rho} + \mathcal{D}^{m}\,, \\ \dfrac{\mathrm{d}(m\boldsymbol{u})}{\mathrm{d}t} &= m\left[-\dfrac{\nabla p}{\rho} + \dfrac{\mathrm{div}\,\mathbb{V}}{\rho} + \boldsymbol{g} + \dfrac{\mathrm{div}(\rho\,\boldsymbol{u}\otimes\delta\boldsymbol{u})}{\rho}\right], \\ \dfrac{\mathrm{d}\boldsymbol{r}}{\mathrm{d}t} &= \boldsymbol{u} + \delta\boldsymbol{u}\,, \quad V = m\,\big/\rho\,, \quad p = c_0^2\,(\rho-\rho_0)\,. \end{cases} \tag{10}$$

Once again we stress that the above equations are derived through a re-shape of the equations (6) and (8). The additional terms $\mathcal{D}^{\rho}$ and $\mathcal{D}^{m}$ represent diffusive contributions and allow to stabilize the numerical scheme when the system (10) is discretized in the SPH fashion. We underline that, without such diffusive terms, we were not able to obtain a stable scheme. Finally, we highlight that the scheme in conservative variables [that is system (9)] and that in primitive variables without diffusive terms [namely system (10) with $\mathcal{D}^{\rho}=0$ and $\mathcal{D}^{m}=0$] are equivalent for continuous solutions of Navier-Stokes equations. The formulation in conservative variables is, however, mandatory if Riemann solvers are used to model the particle interactions (see, for example, Vila [33]).

As discussed above, within the ALE framework $\delta\boldsymbol{u}$ is arbitrary and this can induce large variations on V and m. In fact, while the weakly-compressible assumption implies a constraint on the density field, large variations of $\delta\boldsymbol{u}$ can induce large changes on elementary masses and volumes. To avoid instabilities and inaccuracies, $\delta\boldsymbol{u}$ has therefore to be small in comparison to $\boldsymbol{u}$ and,

similarly to [24], it is only used to regularise the particle distributions. In particular, it is sufficient that $\delta\boldsymbol{u}$ is small in an average sense, i.e. it is allowed to be of order of $\boldsymbol{u}$ locally and in small time intervals but its mean value has to be small in comparison to the actual fluid velocity.

Here, the velocity $\delta\boldsymbol{u}$ is given by a Particle Shifting Technique (hereinafter PST, see [16, 19, 20, 24]) that is conceived to reduce the disorder in the particle distribution and, thus, to improve the accuracy of the discrete differential operators. The velocity $\delta\boldsymbol{u}$ has been made proportional to the smoothing length h so that its magnitude reduces as the spatial resolutions increases. In any case, since $\delta\boldsymbol{u}$ is directly related to the irregularity of the particle distribution, in some conditions its intensity may locally increase in space and time, as better clarified in the next sections. Figure 1 sketches out a description of the above concept. There, the Lagrangian particle trajectory is compared with other three modified trajectories under the action of the PST for three different smoothing lengths. When the smoothing length decreases, the trajectories tends to the Lagrangian one, although there can be significant local deflections. Incidentally, we observe that in some applications purely Lagrangian trajectories may be a drawback of particle methods, since they induce particle clustering along the streamlines and a consequent reduction of accuracy (see [18]). In this case, the shifting algorithm prevents this issue and deviates particles from their Lagrangian paths leading to a regular distribution.

Under the hypothesis that $\delta\boldsymbol{u}$ is small in comparison to the actual velocity field, it is possible to assume that the mass and volume variations remain

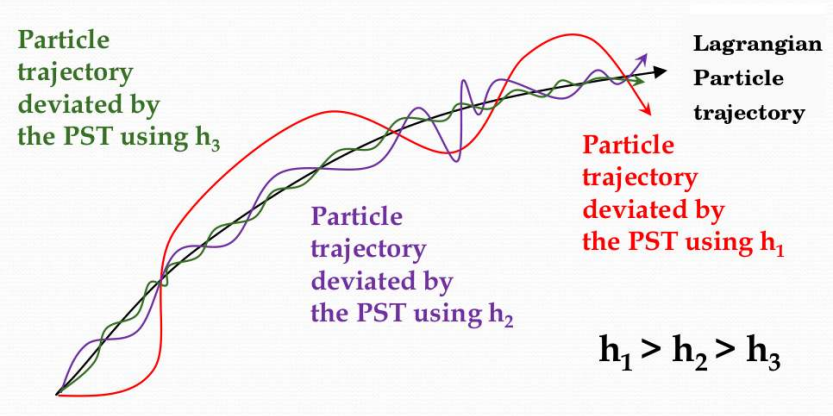

Fig. 1. Sketch of the deviated particles trajectory under the action of a PST using three different smoothing lengths $h_1 > h_2 > h_3$.

small along the modified trajectories (induced by $\delta \boldsymbol{u}$) and the concept of "fluid particle" can be still considered valid. Accordingly, the system (6) can be seen as a "quasi"-Lagrangian formulation. In Section 5 this concept is further exploited.

3 Smoothed differential operators

Before describing the ODEs for the particle system, we briefly introduce the smoothed differential operators used to approximate the right-hand side of equation (10).

In the SPH context the differential operators on the right-hand side of equation (1) are mollified through a suitable convolution integral in the space $\boldsymbol{r}^*$ with a kernel function $W_h(\boldsymbol{r}, \boldsymbol{r}^*)$. The function W_h is assumed to be a positive radial function with a compact support characterized by a reference length h, hereinafter called smoothing length.

Regarding the divergence of the velocity field, the pressure gradient and the

divergence of the viscous stress tensor, they are approximated, for a generic particle i, through the formulas below (see [9, 10]):

$$\begin{cases} \langle \mathrm{div}(\boldsymbol{u}) \rangle_i \;=\; \sum_j \, (\boldsymbol{u}_j \,-\, \boldsymbol{u}_i) \cdot \nabla_i W_{ij} \, V_j \,, \\ \\ \langle \nabla p \rangle_i \;\;\;=\; \sum_j \, (\, p_j \,+\, p_i \,) \, \nabla_i W_{ij} \, V_j \,, \\ \\ \langle \mathrm{div}(\mathbb{V}) \rangle_i \;=\; \mu \, \sum_j \, \pi_{ij} \, \nabla_i W_{ij} \, V_j \,, \\ \\ \pi_{ij} \;\;\;\;\;\;\;=\; K \, \dfrac{(\boldsymbol{u}_j \,-\, \boldsymbol{u}_i) \cdot \boldsymbol{r}_{ji}}{\| \boldsymbol{r}_{ji} \|^2} \,, \end{cases} \tag{11}$$

where $\boldsymbol{r}_{ji} = \boldsymbol{r}_j - \boldsymbol{r}_i$, μ denotes the dynamic viscosity while $K = 2\,(n+2)$ and n is the number of spatial dimensions. About the kernel function, namely $W_{ij} := W_h(\|\boldsymbol{r}_j - \boldsymbol{r}_i\|)$, in this work a C2-Wendland kernel is used and about 50 neighbour particles (in a 2D framework) are considered in the kernel support, which corresponds to $h = 2\Delta x$ where Δx indicates the initial particle distance. In particular, the packing algorithm developed in [11] is used to fill the fluid domain with particles placed in an almost equispaced configuration. The smoothing length h is considered constant in time and space and, therefore, the dependency of W on h is understood in the rest of the work.

As discussed in [9, 10, 25], the smoothed operators in equation (11) approximate the differential operator of equation (1) when both h and $\Delta x/h$ are small. In addition, they allow the conservation of the linear and angular momenta of the discrete particle system as well as the implicitly (in a weak-sense) fulfilment of the dynamic boundary condition at the free-surface.

As discussed in [31], the argument $(p_j + p_i)$ in the pressure term leads to the so-called tensile instability when the pressure field becomes negative. In such a condition the formula can be modified *locally* by using the term $(p_j - p_i)$. This strategy helps removing the tensile instability but introduces an error on the conservation of momenta, which, in any case, can be controlled and limited thanks to the use of the PST.

Finally, the approximation of the terms depending on $\delta\boldsymbol{u}$ (see the system (6)) is performed through the following convolution sums:

$$\boxed{\delta\boldsymbol{u}\text{-terms}} \begin{cases} \langle \mathrm{div}(\delta\boldsymbol{u})\rangle_i & = \displaystyle\sum_j (\delta\boldsymbol{u}_j - \delta\boldsymbol{u}_i)\cdot\nabla_i W_{ij} V_j\,, \\ \langle \mathrm{div}(\rho\delta\boldsymbol{u})\rangle_i & = \displaystyle\sum_j (\rho_j\,\delta\boldsymbol{u}_j + \rho_i\delta\boldsymbol{u}_i)\cdot\nabla_i W_{ij} V_j\,, \\ \langle \mathrm{div}(\boldsymbol{u}\otimes\delta\boldsymbol{u})\rangle_i & = \displaystyle\sum_j (\boldsymbol{u}_j\otimes\delta\boldsymbol{u}_j + \boldsymbol{u}_i\otimes\delta\boldsymbol{u}_i)\cdot\nabla_i W_{ij} V_j\,, \\ \langle \mathrm{div}(\rho\,\boldsymbol{u}\otimes\delta\boldsymbol{u})\rangle_i & = \displaystyle\sum_j (\rho_j\boldsymbol{u}_j\otimes\delta\boldsymbol{u}_j + \rho_i\boldsymbol{u}_i\otimes\delta\boldsymbol{u}_i)\cdot\nabla_i W_{ij} V_j\,. \end{cases} \tag{12}$$

To be consistent, the divergence of $\delta\boldsymbol{u}$ is evaluated by using the same formula adopted for the divergence of the velocity (11). Conversely, the other divergence operators are expressed through a sum instead of a difference. Indeed, the symmetric behaviour when swapping the indexes i and j allows to derive terms which conserve the mass and the linear momentum of the particle system, as shown in the next section.

4 The discrete particle system

Using the SPH approximation introduced in Section 3, the differential equation for the particle system can be derived by approximating the right-hand side of the equation (10) as follows:

$\boxed{\delta\text{-ALE-SPH}}$

$$\begin{cases} \dfrac{\mathrm{d}\rho_i}{\mathrm{d}t} &= -\rho_i \langle \mathrm{div}(\boldsymbol{u} + \delta\boldsymbol{u})\rangle_i + \langle \mathrm{div}(\rho\delta\boldsymbol{u})\rangle_i + \mathcal{D}_i^{\rho}\,, \\ \dfrac{\mathrm{d}m_i}{\mathrm{d}t} &= m_i \dfrac{\langle \mathrm{div}(\rho\,\delta\boldsymbol{u})\rangle_i}{\rho_i} + \mathcal{D}_i^{m}\,, \\ \dfrac{\mathrm{d}(m_i\,\boldsymbol{u}_i)}{\mathrm{d}t} &= -m_i \dfrac{\langle \nabla p\rangle_i}{\rho_i} + m_i \dfrac{\langle \mathrm{div}(\mathbb{V})\rangle_i}{\rho_i} + \\ & \quad + m_i \dfrac{\langle \mathrm{div}(\rho\,\boldsymbol{u} \otimes \delta\boldsymbol{u})\rangle_i}{\rho_i} + m_i\boldsymbol{g}\,, \\ \dfrac{\mathrm{d}\boldsymbol{r}_i}{\mathrm{d}t} &= \boldsymbol{u}_i + \delta\boldsymbol{u}_i, \quad V_i = m_i \,/\rho_i, \quad p = c_0^2(\rho - \rho_0), \end{cases} \tag{13}$$

where $\mathcal{D}_i^{\rho}$ is the numerical diffusive term introduced by [4] to filter-out the spurious high-frequency noise in the pressure field. Conversely, $\mathcal{D}_i^{m}$ is the diffusive term in the mass equation. These terms are modelled as follow:

$$\begin{cases} \mathcal{D}_i^{m} &= 2\delta h c_0 \sum\limits_j (m_j - m_i)\,\mathcal{F}_{ij}\,\sqrt{V_i\,V_j}\,, \\ \mathcal{D}_i^{\rho} &= 2\delta h c_0 \sum\limits_j \psi_{ji}\,\mathcal{F}_{ij}\,V_j\,, \\ \psi_{ji} &= (\rho_j - \rho_i) - \tfrac{1}{2}\left[\langle\nabla\rho\rangle_i^L + \langle\nabla\rho\rangle_j^L\right]\cdot\boldsymbol{r}_{ji}\,, \\ \mathcal{F}_{ij} &= \dfrac{\boldsymbol{r}_{ji}\cdot\nabla_i W_{ij}}{\|\boldsymbol{r}_{ji}\|^2}\,, \end{cases} \tag{14}$$

where δ is set equal to 0.1 (see, for example, [6]) and the superscript L indicates that the gradient is evaluated through the renormalized gradient equation, *i.e.*:

$$\langle \nabla \rho \rangle_i^L = \sum_j (\rho_j - \rho_i)\, \mathbb{L}_i^{-1}\, \nabla_i W_{ij}\, V_j\,, \qquad \mathbb{L}_i := \left[\sum_k (\boldsymbol{r}_j - \boldsymbol{r}_k) \otimes \nabla_i W_{ik}\, V_k \right] \quad (15)$$

where $\mathbb{L}_i$ is the renormalization matrix (see *e.g* [2]).

The initial mass distribution is obtained from the initial density (pressure) field and the initial volume distribution, namely $m_i(t_0) = \rho_i(t_0)\, V_i(t_0)$. Then, the masses evolve with their own equation.

Differently from [28] where the Particle Shifting Technique (PST) was implemented as a particle shifting displacement (namely $\delta \boldsymbol{r}$), in the present work the PST is written in terms of velocity deviation $\delta \boldsymbol{u}$, that is:

$$\delta \boldsymbol{u}_i = \min \left(\|\delta \boldsymbol{u}_i^*\|\,, \frac{U_{\max}}{2} \right) \frac{\delta \boldsymbol{u}_i^*}{\|\delta \boldsymbol{u}_i^*\|} \quad (16)$$

where U_{max} is the maximum expected velocity and $\delta \boldsymbol{u}_i^*$ is given below:

$$\delta \boldsymbol{u}_i^* = -\mathrm{Ma}\,(2h)\, c_0 \sum_j \left[1 + R \left(\frac{W_{ij}}{W(\Delta x)} \right)^n \right] \nabla_i W_{ij} V_j\,. \quad (17)$$

Here, $\mathrm{Ma} = U_{\max}/\, c_0$ and the constants R and n are respectively set to 0.2 and 4 as in [28, 32]. Incidentally, we highlight that the proposed model is only weakly influenced by variations of the parameters R and n. Equation (16) is introduced to limit the magnitude of the shifting velocity. Since formula (17) is proportional to the smoothing length, the intensity of $\delta \boldsymbol{u}$ reduces as the spatial resolution increases and this guarantees that the hypothesis made in the previous section (i.e., $\delta \boldsymbol{u}_i$ induces small deviations with respect to the physical particle trajectory) is valid.

As documented in [28], the use of the PST leads to regular particle distributions and increases the accuracy and the robustness of the scheme. In turn, a direct inclusion of the PST causes the loss of the conservation of linear and angular momenta (even though the discrepancies from the exact conservation remain small during the evolution). Differently from the scheme proposed in [28], in the following section we prove that the additional terms depending on $\delta\boldsymbol{u}$ allow for a better conservation of total volume and reduce those inconsistencies that can lead to wrong solutions, especially in presence of confined domains.

4.1 Mass, momenta and volume conservation for the δ-ALE-SPH scheme

In the present section we show how the use of a velocity deviation $\delta\boldsymbol{u}$ influences the main conservation properties of the scheme. To this purpose, we consider a particle system consisting of only fluid particles (no solid boundaries).

If we apply the summation all over the particles to the second equation of system (13), we obtain the following time derivative of the total mass:

$$\frac{\mathrm{d}}{\mathrm{d}t}\sum_i m_i = \sum_i \left[V_i \left\langle \mathrm{div}(\rho\,\delta\boldsymbol{u}) \right\rangle_i + \mathcal{D}_i^m \right]. \tag{18}$$

Let us focus on the right-hand side. Since the inner arguments of $V_i \left\langle \mathrm{div}(\rho\,\delta\boldsymbol{u}) \right\rangle$ and $\mathcal{D}^m$ are antisymmetric with respect the swapping of the indices i-j, the double summations contain contributions equal in magnitude and opposite in sign that cancel out exactly. Consequently, the right-hand side of the equation (18) is identically null and this implies the conservation of the global mass of the fluid system.

A similar procedure can be applied to the continuity equation, namely the first

equation of the system (13), showing that the terms $\langle \mathrm{div}(\rho\,\delta\boldsymbol{u})\rangle$ and $\mathcal{D}_i^{\rho}$ give a null contribution to the global fluid system thanks to their symmetric structure. This proves that the discrete equation is consistent with the global continuity equation without diffusion and velocity deviations.

As already explained above, the pressure and the viscous forces [namely, the second and third equation of equation (11)] conserve both linear and angular momenta. Then, for the linear momentum, we obtain:

$$\frac{\mathrm{d}}{\mathrm{d}t}\sum_i (m_i\,\boldsymbol{u}_i) \;=\; \sum_i \left[m_i\boldsymbol{g}_i + \langle \mathrm{div}(\rho\boldsymbol{u}\otimes\delta\boldsymbol{u})\rangle_i V_i\right]. \tag{19}$$

Again, thanks to the symmetric structure of $\langle \mathrm{div}(\rho\,\boldsymbol{u}\otimes\delta\boldsymbol{u})\rangle$, this term gives a null contribution and, consequently, the linear momentum of the particle system is preserved.

On the contrary, if we consider the angular momentum of the particles system, we obtain:

$$\frac{\mathrm{d}}{\mathrm{d}t}\sum_i(\boldsymbol{r}_i\times m_i\boldsymbol{u}_i) = \sum_i\left[\boldsymbol{r}_i\times m_i\boldsymbol{g}_i + \boldsymbol{r}_i\times\langle \mathrm{div}(\rho\boldsymbol{u}\otimes\delta\boldsymbol{u})\rangle_i V_i\right] \tag{20}$$

and the summation of the last term on the right-hand side is not identically zero. This is caused by the fact that the argument of $\langle \mathrm{div}(\rho\boldsymbol{u}\otimes\delta\boldsymbol{u})\rangle_i V_i$ is not radial (i.e. proportional to $\boldsymbol{r}_{ji}$). This implies that within the ALE framework the conservation of the angular momentum is lost. In any case, as shown in [28], the benefits of the PST on the solution accuracy are higher than this drawback, and, moreover, the error on the angular momentum conservation reduces when the smoothing length h decreases.

Under the assumption of weak-compressibility, the volume of the fluid domain is allowed to change by 1%. However, if we consider hydrodynamic problems where the

fluid is confined by non-moving solid boundaries and/or periodic boundaries, the volume domain Ω remains constant, that is $\int_\Omega \mathrm{div}(\boldsymbol{u})dV = \int_{\partial\Omega} \boldsymbol{u}\cdot\boldsymbol{n} = 0$. Combining the first two equations of system (13), we obtain the time derivative of the global volume of the particle system:

$$\frac{\mathrm{d}}{\mathrm{d}t}\sum_i V_i \;=\; \sum_i \left[\, V_i \,\langle \mathrm{div}(\boldsymbol{u}+\delta\boldsymbol{u})\rangle_i \;+\; \frac{\mathcal{D}_i^m}{\rho_i} \;-\; \frac{V_i\,\mathcal{D}_i^\rho}{\rho_i} \,\right]. \tag{21}$$

Since the right-hand side is generally different from zero (even in the absence of diffusive terms and of the $\delta\boldsymbol{u}$-term), the conservation of the total volume of Ω is not guaranteed. In particular, this occurs in all the weakly compressible SPH models (i.e. the mass conservation is ensured but not the volume one, see for example [15]). About the present scheme, the smoothed operators in Eq. (21) imply that the contributions generated by the addition of the $\delta\boldsymbol{u}$-terms and by the diffusive terms reduce as h decreases (namely, as the spatial discretization becomes finer).

5 Two alternative variants: particles with constant mass or constant volumes

Since the shifting velocity is proportional to h, we can simplify the system of equations by assuming that the particle mass does not change along the path $(\boldsymbol{u}+\delta\boldsymbol{u})$. The error induced by such an approximation is expected to be small and to reduce when increasing the spatial resolution (*i.e.* $h \to 0$), as already explained in Section 2.3. Under this hypothesis the particle volumes are directly linked to their densities through the relation:

$$V_i(t) \;=\; m_i/\rho_i(t) \tag{22}$$

and the mass conservation is intrinsically satisfied as in the standard SPH model. Because of the above link between volume, mass and density, the ALE framework is not more necessary and we can directly discretize the system (6). Then, the equations for this first variant becomes:

Scheme with constant masses

$$\begin{cases} \dfrac{\mathrm{d}\rho_i}{\mathrm{d}t} = -\rho_i \langle \mathrm{div}(\boldsymbol{u} + \delta\boldsymbol{u}) \rangle_i + \langle \mathrm{div}(\rho \delta\boldsymbol{u}) \rangle_i + \mathcal{D}_i^{\rho} \\ \dfrac{\mathrm{d}\boldsymbol{u}_i}{\mathrm{d}t} = -\dfrac{\langle \nabla p \rangle_i}{\rho_i} + \dfrac{\langle \mathrm{div}\, \mathbb{V} \rangle_i}{\rho_i} + \boldsymbol{g} + \langle \mathrm{div}(\boldsymbol{u} \otimes \delta\boldsymbol{u}) \rangle_i - \boldsymbol{u}_i \langle \mathrm{div}(\delta\boldsymbol{u}) \rangle_i \\ \dfrac{\mathrm{d}\boldsymbol{r}_i}{\mathrm{d}t} = \boldsymbol{u}_i + \delta\boldsymbol{u}_i\,, \quad V_i(t) = m_{0i} \,/ \rho_i(t), \quad p = c_0^2 \left(\rho - \rho_0\right). \end{cases} \tag{23}$$

which coincides with the consistent derivation of the δ^+-SPH model described in Sun et al. [29]. In that work it is underlined that the action of the $\delta\boldsymbol{u}$-terms is problem dependent and that the terms in the continuity equation are more relevant than those in the momentum equation which play a negligible role. In particular, in the first benchmark of Section 6 all the $\delta\boldsymbol{u}$-terms have irrelevant effects, while in the remaining benchmarks they are of fundamental importance to avoid a non-physical drift on the volume conservation.

A second possible variant is obtained by enforcing that the particle volumes do not change. Indeed the PST guarantees an ordered spatial particle distribution during all the time evolution and, therefore, we can assume that the particle volumes remain close to the initial ones, *i.e* $dV_i/dt = 0$. Following this second approximation, the conservation of total volume is intrinsically enforced, while the particle masses are given by:

$$m_i(t) = V_{0i}\, \rho_i(t) \tag{24}$$

The equations for the density and the momentum are derived by discretizing the system (6) through the smoothing procedure described in Section 3:

Scheme with constant volumes

$$\begin{cases} \dfrac{\mathrm{d}\rho_i}{\mathrm{d}t} \;=\; -\rho_i \prec\!\mathrm{div}(\boldsymbol{u}+\delta\boldsymbol{u})\!\succ_i + \prec\!\mathrm{div}(\rho\delta\boldsymbol{u})\!\succ_i + \mathcal{D}_i^{\rho} \\ \dfrac{\mathrm{d}\boldsymbol{u}_i}{\mathrm{d}t} \;=\; -\dfrac{\prec\!\nabla p\!\succ_i}{\rho_i} + \dfrac{\prec\!\mathrm{div}\,\mathbb{V}\!\succ_i}{\rho_i} + \boldsymbol{g} + \prec\!\mathrm{div}(\boldsymbol{u}\otimes\delta\boldsymbol{u})\!\succ_i - \boldsymbol{u}_i \prec\!\mathrm{div}(\delta\boldsymbol{u})\!\succ_i \\ \dfrac{\mathrm{d}\boldsymbol{r}_i}{\mathrm{d}t} \;=\; \boldsymbol{u}_i + \delta\boldsymbol{u}_i\,, \quad m_i(t) = V_{0i}\,\rho_i(t), \quad p = c_0^2\,(\rho-\rho_0)\,. \end{cases} \tag{25}$$

It this worth noting that, differently from the scheme (23), the smoothed operators in (25) are evaluated by using the volumes V_{0j} during all the simulation. The same procedure is used for the shifting velocity defined in equation (17). For the above reason, the smoothed operators in (25) are indicated through the symbol $\prec\!\succ$ and, for example, the divergence operator is rewritten as:

$$\prec\!\mathrm{div}(\boldsymbol{u})\!\succ_i = \sum_j (\boldsymbol{u}_j - \boldsymbol{u}_i)\cdot\nabla_i W_{ij}\,V_{0j}\,. \tag{26}$$

In the next section we will show that the results given by these two variants are practically the same and very close to those obtained though the δ-ALE-SPH. We stress that, strictly speaking, the above variants cannot be regarded as ALE schemes on their own.

6 Numerical results

In order to validate the δ-ALE-SPH model, namely the system (13), we consider the same benchmark used in the works [12] and [28], concerning the viscous flow past an inclined elliptical cylinder in subsection 6.1, and the lid-driven cavity problem for two Reynolds numbers in subsection 6.2. Finally, in subsection 6.3 we consider the evolution of a dam-break flow impacting a vertical wall.

6.1 The flow past an inclined elliptical cylinder with an angle of attack of 20° at Re = 500

In this subsection the viscous flow past an inclined elliptical cylinder is considered. The chord length of the profile is the major axis of the ellipse and it is indicated in the following text with the letter a. The ratio between the axes is equal to $b/a = 0.4$ and the angle of attack is $\alpha = 20°$. The Reynolds number is $Re = aU/\nu = 500$, where U is the upstream horizontal velocity and ν the kinematic viscosity.

Colagrossi et al.[12] showed that δ-SPH model is able to evaluate the forces acting on the inclined ellipse in a good accordance with a reference solution obtained with a vortex method, i.e. the Diffusive Vortex Hydrodynamic (DVH) model [26]. Despite this, the vorticity field was affected by numerical noise induced by the particles' spatial disorder. In [27, 28] it was shown that the use of the PST allows for a better evaluation of the vorticity field, also improving the accuracy on the global force evaluation.

Figure 2 shows the pressure and vorticity fields evaluated with the δ-ALE-SPH model at the final time of the simulation, namely $tU/a = 50$, when a periodic

regime of the solution is attained. Figure 3 depicts the time histories of the viscous component in drag force obtained for three different spatial resolutions, namely $a/\Delta x = 25, 50, 100$. These results are compared with the reference solution given by the DVH model, showing that the δ-ALE-SPH converges to the DVH output and proving that the boundary layer is correctly resolved by this SPH variant.

Figure 4 depicts the volume distribution given by the δ-ALE-SPH model by using three different spatial resolutions, that is $a/\Delta x = 25, 50, 100$. The contour plots refer to the field of relative volume variations, i.e. $\epsilon_{Vi} = (V_i/V_0 - 1)$, where V_0 is the initial particle volume. Since for this problem the initial configuration is a uniform Cartesian lattice, the initial volumes are all equal to $V_0 = \Delta x^2$. The relative volume variations are of the order of few percentage and, furthermore, they reduce when $a/\Delta x$ increases. This is due to the fact that the shifting velocity $\delta \boldsymbol{u}$ becomes smaller

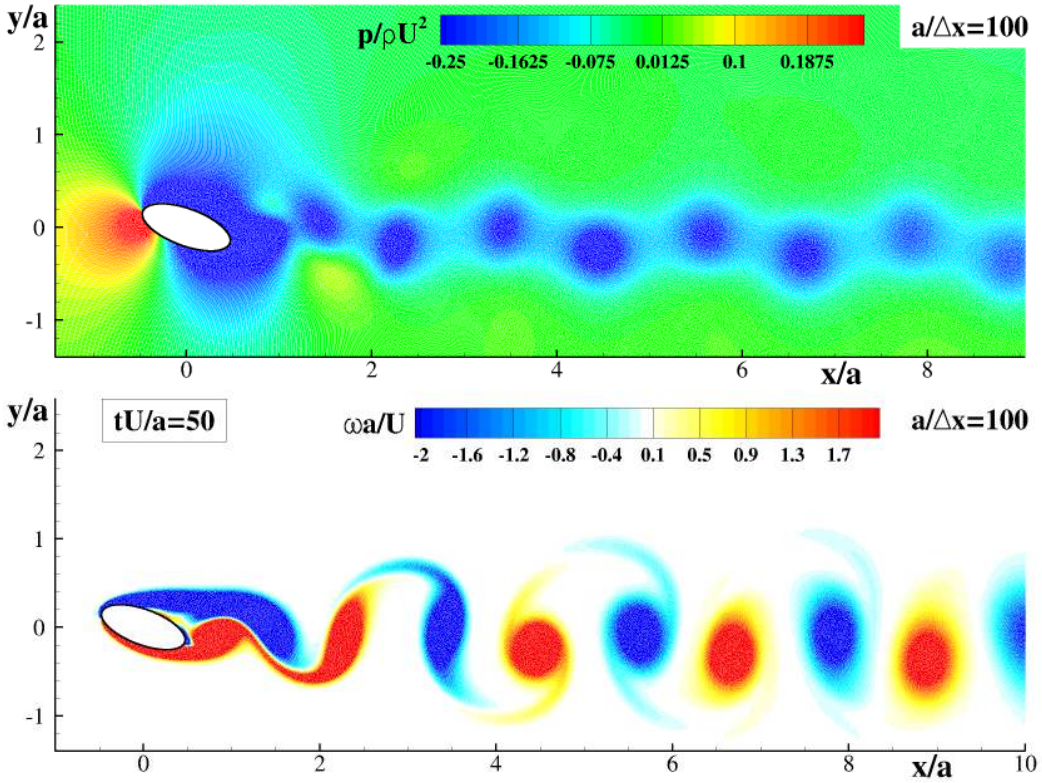

Fig. 2. The flow past an inclined elliptical cylinder at $tU/a = 50$ for $a/\Delta x = 100$. The pressure (top) and vorticity (bottom) fields predicted by the δ-ALE-SPH.

when h decreases (note that $h/\Delta x = 2$ for all the simulations). On the other hand, the field ϵ_{Vi} becomes more and more irregular when $a/\Delta x$ increases.

The above results indirectly show that the hypothesis on the behaviour of $\delta\boldsymbol{u}$ done in the previous sections are basically satisfied. The shifting velocity can present local irregularities caused by the particles' disorder, but, in any case, their magnitude tends to reduce with the particle sizes.

In Figure 5 the particle mass distribution is shown for the highest resolution, that is $a/\Delta x = 100$. The contour plot refers to field of the relative mass variations, i,e, $\epsilon_{mi} = (m_i/m_0 - 1)$, where m_0 are the initial particle masses evaluated as $m_0 = \rho_0 \Delta x^2$. The mass variations ϵ_{mi} present a pattern which is essentially similar to the ϵ_{Vi} distribution. This behaviour is likely due to the fact that the density field is much more regular than both V_i and m_i and, consequently, ϵ_{mi} and ϵ_{Vi} are closely related.

The left plot of Figure 6 reproduces an enlarged view of the field ϵ_{Vi} for $a/\Delta x = 25$, while the right plot displays the simulation with $\mathcal{D}^m$ set to zero. When the mass diffusion is inhibited, the scheme becomes unstable, leading to large variations of ϵ_{Vi}

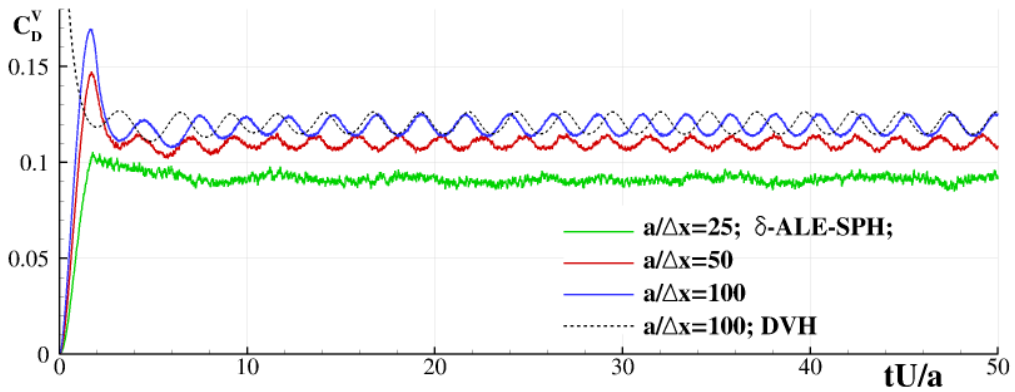

Fig. 3. The flow past an inclined elliptical cylinder. Time histories of the viscous drag component predicted by the δ-ALE-SPH for three different resolutions: $a/\Delta x = 25, 50, 100$. The dashed black line is the solution given by the DVH model (see [26]).

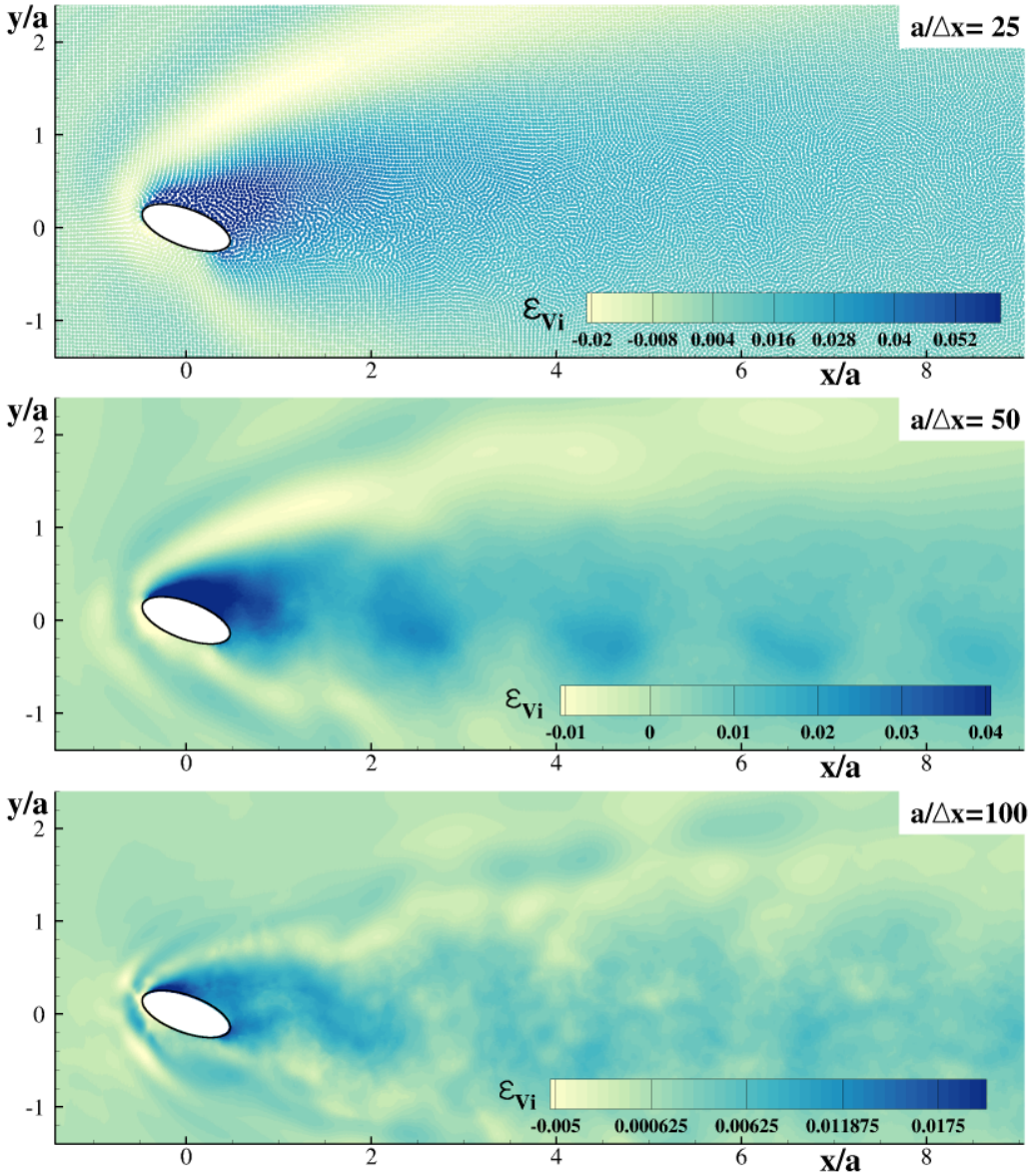

Fig. 4. The flow past an inclined elliptical cylinder. Particle volume distributions predicted through the δ-ALE-SPH for three spatial resolutions, namely $a/\Delta x = 25, 50, 100$.

(up to 50%). After that, the mass and volume variations continue to increase because the errors induced on the smoothed operators are enlarged by the inhomogeneous particle distribution. For this reason the simulation is stopped at time $tU/c = 2.5$. From a theoretical point of view, the cause of this instability is still unknown and deserves a future investigation.

For the test-case selected in this work, the volume of the fluid domain is constant

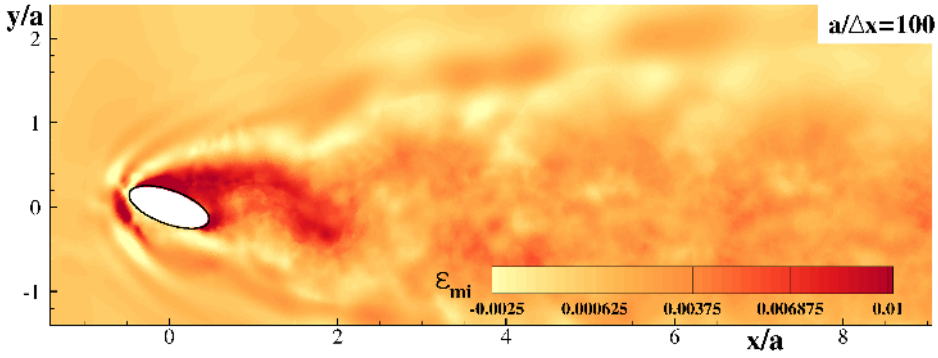

Fig. 5. The flow past an inclined elliptical cylinder. Particle mass distributions predicted by δ-ALE-SPH for $a/\Delta x = 100$.

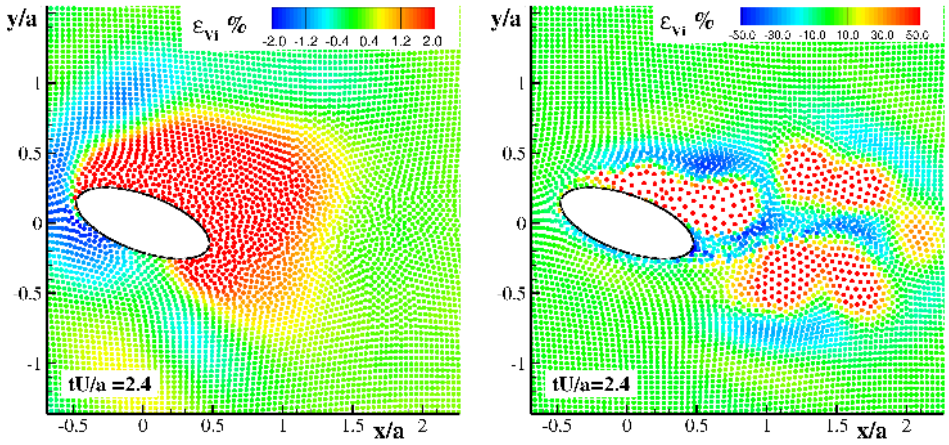

Fig. 6. The flow past an inclined elliptical cylinder for $a/\Delta x = 25$. Contour plots of the relative variation of the particle volumes with respect to their initial value, namely ϵ_{Vi}. Left: a regular particle distribution obtained through the δ-ALE-SPH. Right: numerical instability using the δ-ALE-SPH without the diffusion term $\mathcal{D}^m$.

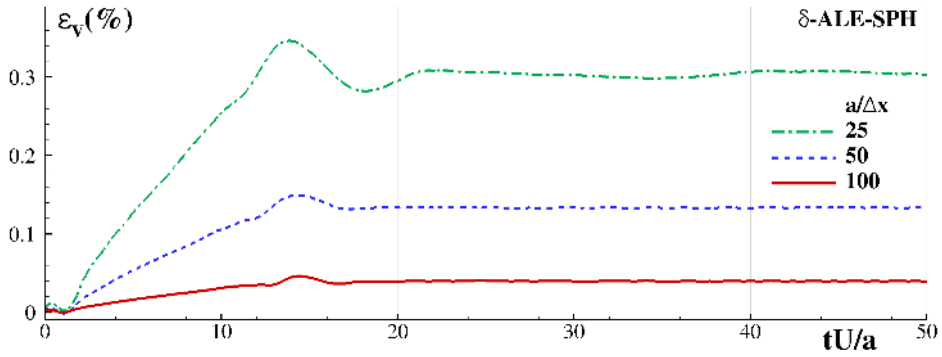

Fig. 7. The flow past an inclined elliptical cylinder for $a/\Delta x = 25, 50, 100$. Time history of the relative variation of the total particle volume, namely $\epsilon_{\mathcal{V}}$ in Eq. (27), predicted by the δ-ALE-SPH.

and equal to $14c \times 10c = 140c^2$. Figure 7 shows the time history of $\epsilon_{\mathcal{V}}$ defined as:

$$\epsilon_{\mathcal{V}} = \frac{\sum_i V_i}{\sum_i V_{0i}} - 1 \tag{27}$$

evaluated by the δ-ALE-SPH model for three spatial resolutions, i.e. $a/\Delta x = 25, 50, 100$. As expected, $\epsilon_{\mathcal{V}}$ reduces when resolution increases and, consequently, $\sum_i V_i$ converges to the geometrical volume of the fluid domain.

Benchmark N°1 solved with constraints on particle masses and volumes

In this section we consider the two variants of the δ-ALE-SPH described in Section 5, namely the constant-mass scheme in equation (23) and the constant-volume model in (25). Figure 8 displays the time history of the drag coefficient evaluated by the different models (the results from the complete δ-ALE-SPH are also displayed). These models yield practically the same results which are all in a good agreement with the reference solution reported in [12] for the same test-case. The same behaviour is observed for the other force components (the velocity and the pressure field are not shown here for the sake of brevity).

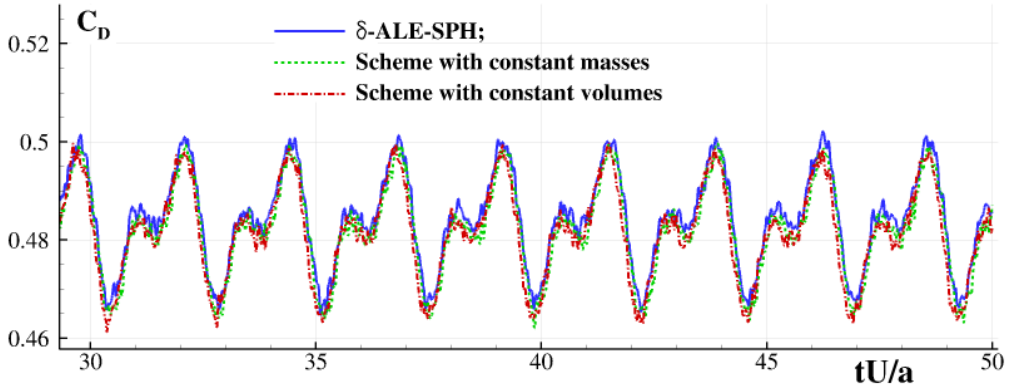

Fig. 8. The flow past an inclined elliptical cylinder for $a/\Delta x = 100$. Time histories of the drag coefficient using the δ-ALE-SPH scheme and the simplified versions described in equations (23) and (25).

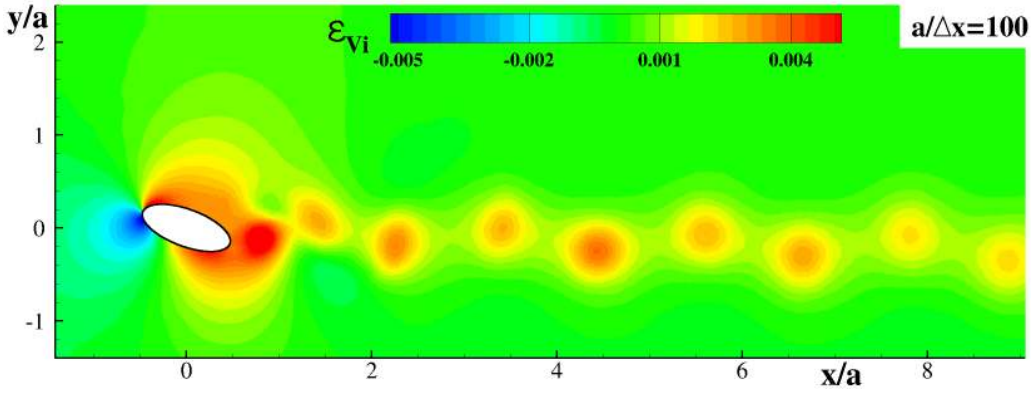

Fig. 9. The flow past an inclined elliptical cylinder for $a/\Delta x = 100$. Contour plot of the relative volume variations ϵ_{Vi} as predicted by the scheme with constant masses [see equation (23)].

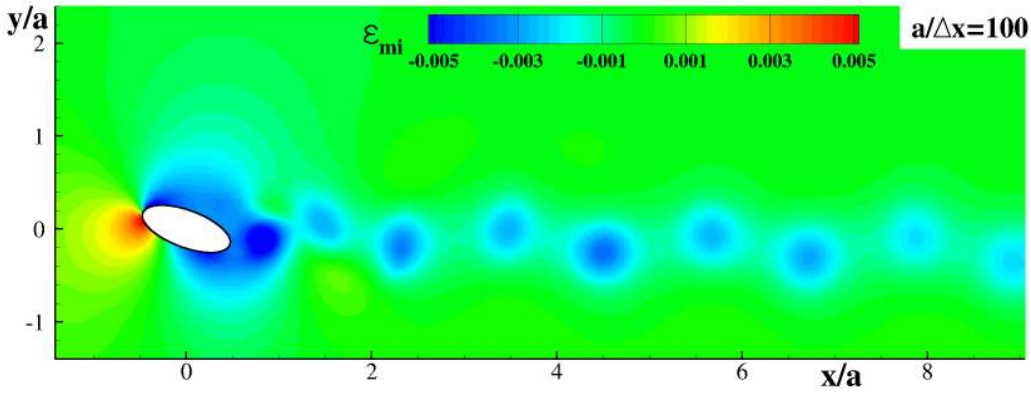

Fig. 10. The flow past an inclined elliptical cylinder for $a/\Delta x = 100$. Contour plot of the relative mass variations ϵ_{mi} as predicted by the scheme with constant volumes [see equation (25)].

Even though both the variants have not large effects on forces, velocity and pressure fields, the mass and volume distributions are different with respect to those given by the δ-ALE-SPH. The volume distribution for the SPH variant where the masses are forced to be constant in time is shown in Figure 9. As already commented above, the constraint on the masses implies that the volumes share the same pattern of the pressure/density field. A similar behaviour is observed when the volumes are enforced to be constant in time: indeed, in a such condition, the mass distribution follows the pressure/density field (see Figure 10). For this reason and because of the weakly-compressibility assumption, the variations on the masses are limited within

the 1%, i.e.

$$\frac{\Delta m_i}{m_0} = \frac{\Delta \rho_i}{\rho_0} \leq 0.01 \tag{28}$$

The same applies to volumes when the constraint on the masses is used.

6.2 Lid-driven cavity at Re = 100 and Re=1000

As a second benchmark we consider the lid-driven cavity problem. This consists of a two-dimensional squared domain with fixed solid walls along three sides and a wall moving tangentially at constant velocity U on the top side. As usual, the Reynolds number is given by $\mathrm{Re} = UL/\nu$ where L is the square side and ν is the kinematic viscosity of the fluid. In particular, we consider the motion at $\mathrm{Re} = 100$ and $\mathrm{Re} = 1000$. In both the cases, the dynamics reach a steady state after a transient whose duration depends on the specific Reynolds number.

Being the domain a simple square the ghost-particle approach [8] is chosen to enforce the no-slip condition. It worth to note that within this technique it is important to mirror also the $\delta\boldsymbol{u}$ field along with the velocity and pressure fields, in order to impose the condition $\delta\boldsymbol{u} \cdot \boldsymbol{n} = 0$ on the solid surfaces. For the velocity field, as explained in [13] and further in [7], a different mirroring is required for the continuity and momentum equations.

Figure 11 shows the steady state solutions obtained through the proposed δ-ALE-SPH model for both the Reynolds numbers. In particular, the left panels display the pressure field and the streamlines while the right panels show the vorticity field. The main difference between $\mathrm{Re} = 100$ and $\mathrm{Re} = 1000$ is represented by the generation in the latter case of a large central vortex and of larger re-circulations regions close to the bottom corners. In both the cases the use of the PST allows for

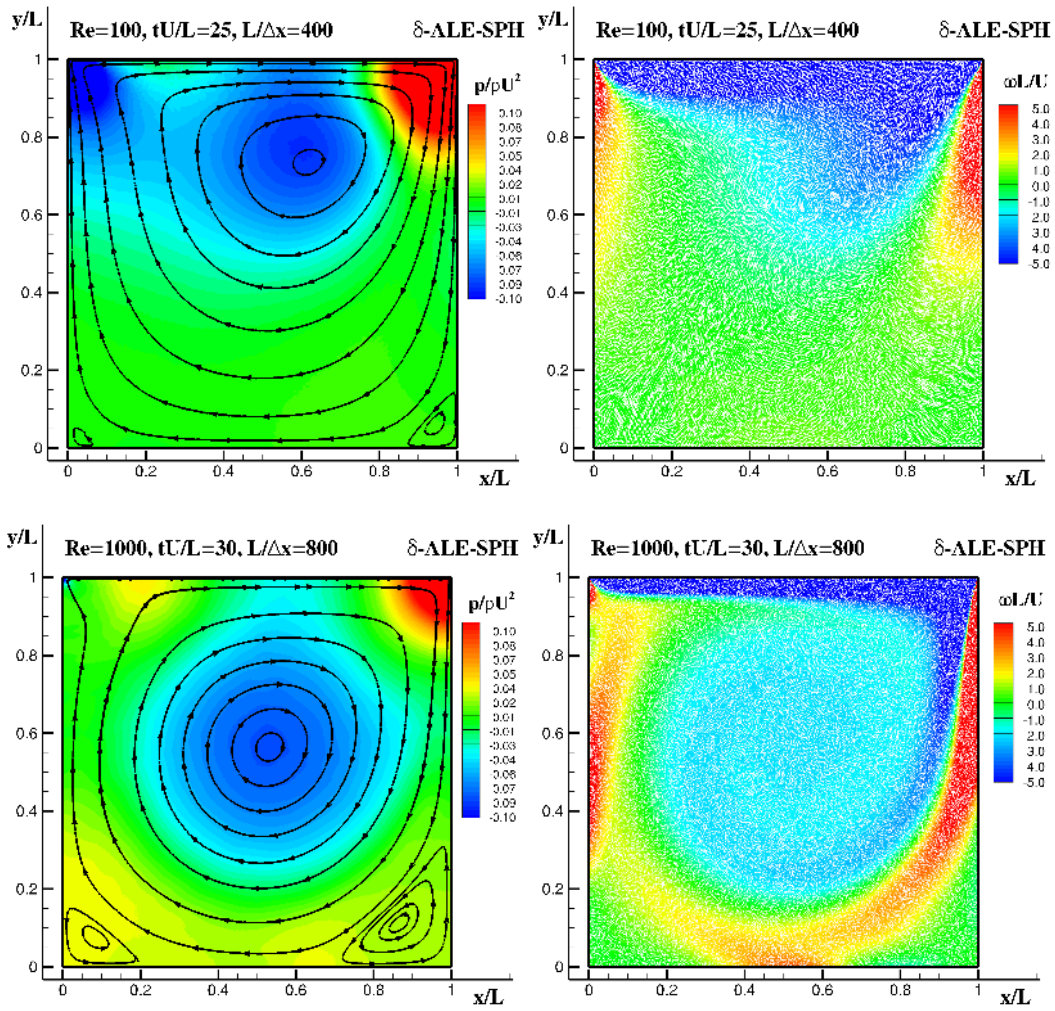

Fig. 11. Lid-driven cavity at $Re = 100$ (top panels) and $Re = 1000$ (bottom panels). Left: pressure field and streamlines. Right: vorticity field.

very regular solutions and avoids the onset of any spurious numerical noise, which, on the contrary, affects SPH models where PST are not used.

In order to validate the proposed method on this second benchmark, Figure 12 displays the comparisons between the results of δ-ALE-SPH model, the results described in Xu et al. [34] and the solution obtained through the consistent δ^+-SPH model of Sun et al. [29] (that is, the mass-constant variant of the δ-ALE-SPH model in Section 5) when the steady state is attained. In particular, the left panels provide the solutions for the horizontal velocity component u at $x = 0.5L$, the middle panels the vertical velocity component v at $y = 0.5L$ and the right panels

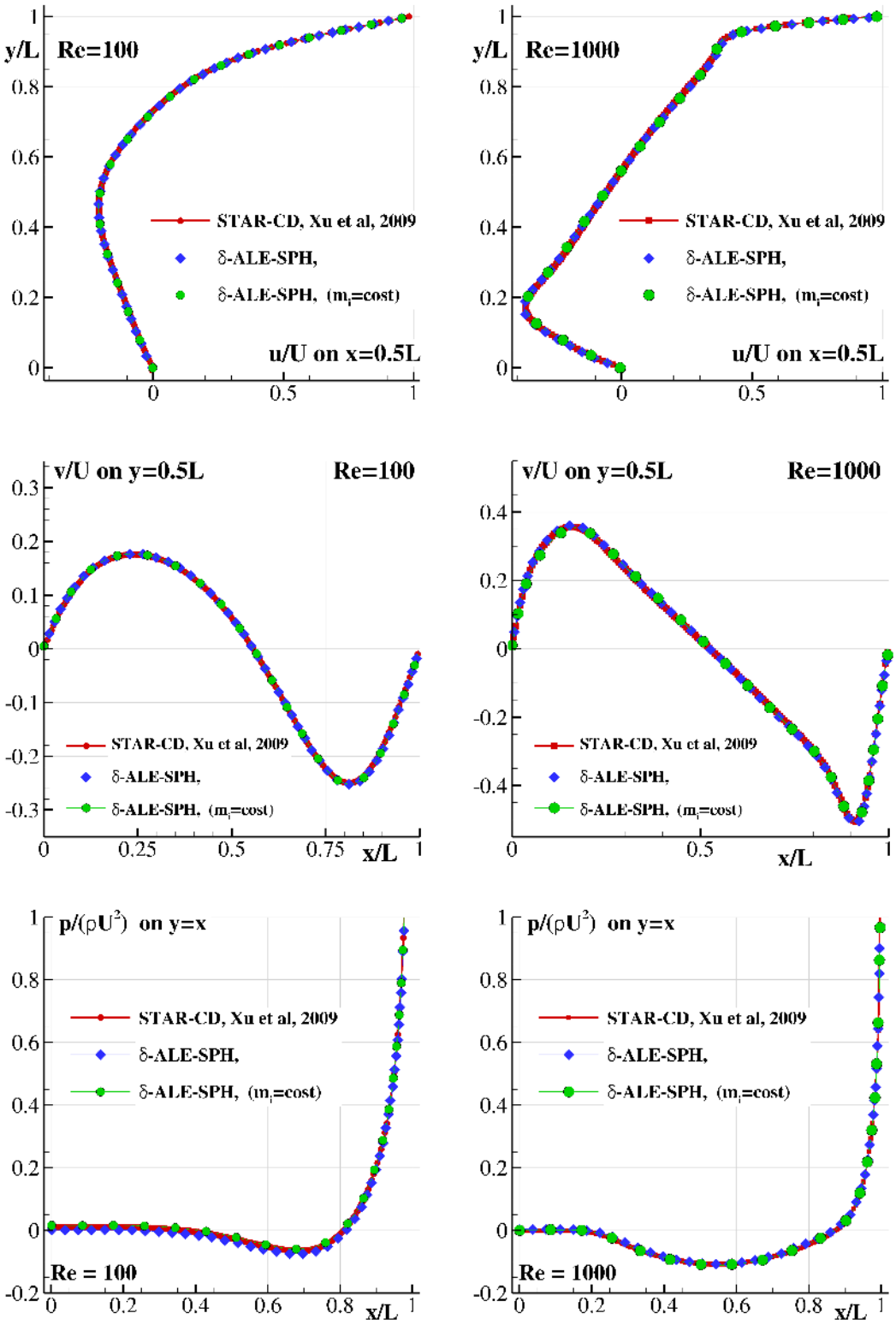

Fig. 12. Lid-driven cavity at $Re = 100$ (left panels) and $Re = 1000$ (right panels). Comparisons between the results of δ-ALE-SPH model, the reference results described in Xu et al. [34] and the solution obtained through the *consistent* δ^+-SPH model of Sun et al. [29]. Top: the horizontal velocity component u along $x = 0.5L$. Middle: the vertical velocity component v along $y = 0.5L$. Bottom: the pressure along the axis $x = y$.

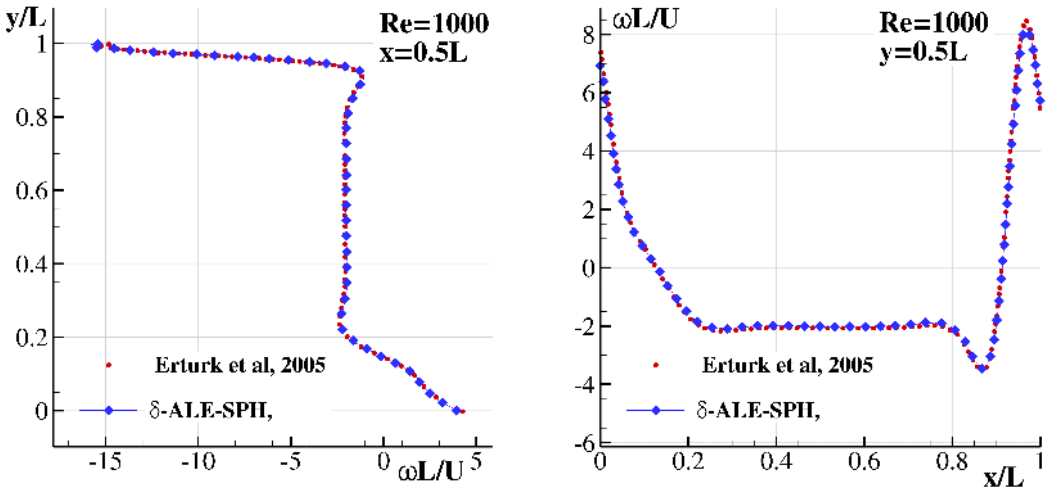

Fig. 13. Lid-driven cavity at $Re = 1000$. Comparisons between the results of δ-ALE-SPH model and the reference results described in [14]. Left: vorticity ω along $x = 0.5L$. Right: vorticity ω along $y = 0.5L$

display the pressure along the diagonal $x = y$. The spatial resolutions are the same indicated in Figure 11. For both the Reynolds numbers the agreement between the different solvers is very good, confirming the accuracy of the proposed model as well as the fact that the equation of the particle's mass variations in Eq. (13) is not crucial in terms of the obtained results.

A further validation is depicted in Figure 13 where the comparisons between δ-ALE-SPH model and the results presented in Erturk et al. [14] are shown in terms of the vorticity field evaluated along the line $x = 0.5L$ and $y = 0.5L$ at the steady condition.

The most challenging issue related to the numerical solution of the lid-driven cavity is represented by the singularities that occur at the top-right and top-left corners of the squared domain. There, the no-slip condition is ill-defined since $\boldsymbol{u} = 0$ along the side wall and $\boldsymbol{u} = U\boldsymbol{e}_1$ along the top wall, introducing a discontinuity on the domain boundary. In the numerical simulation this twofold assignment is the cause of errors in the particle volume evolution. With respect to this, Figure 14 displays

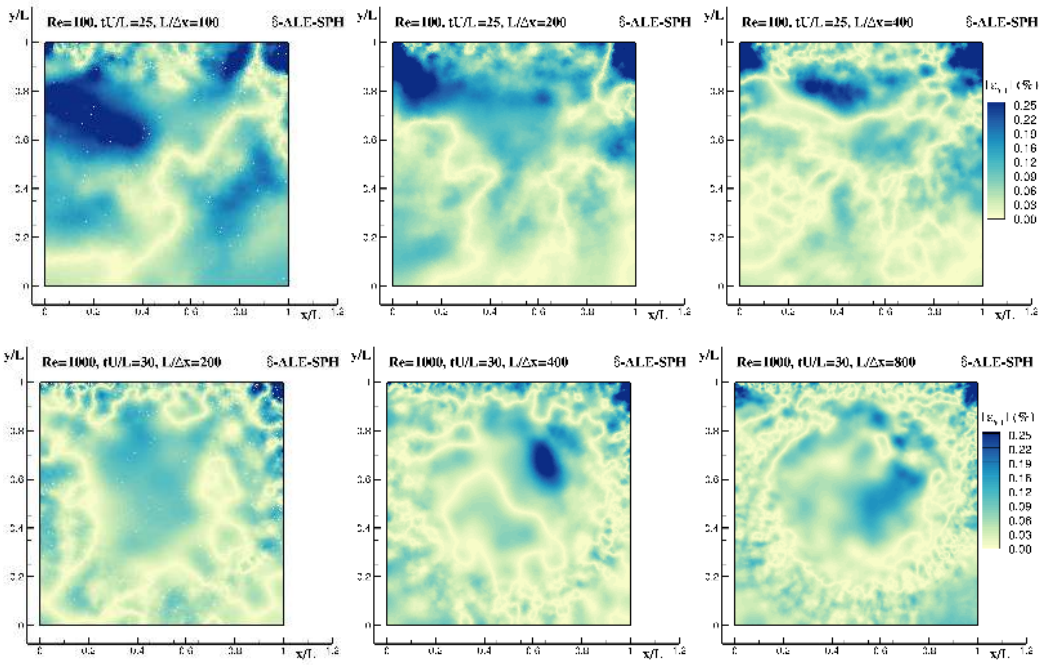

Fig. 14. Lid-driven cavity at $Re = 100$ (top panels) and $Re = 1000$ (bottom panels). Snapshots of the evolution of $|\epsilon_{Vi}|$ at different spatial resolutions for the δ-ALE-SPH model.

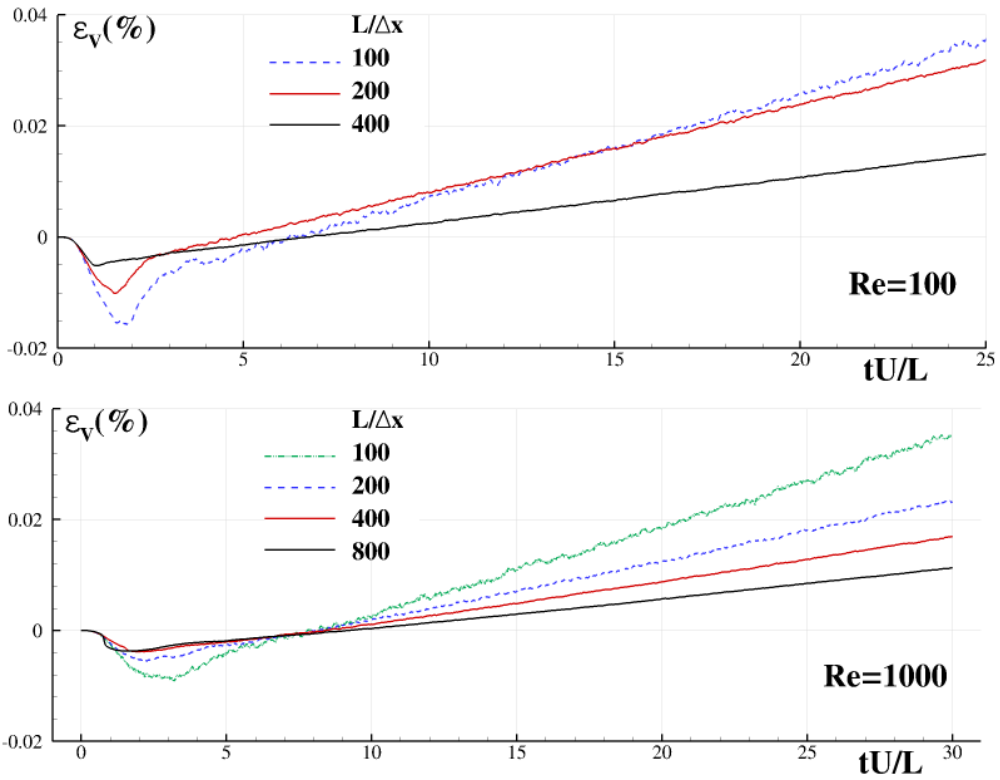

Fig. 15. Lid-driven cavity at $Re = 100$ (top panels) and $Re = 1000$ (bottom panels). Time histories of ϵ_V for different spatial resolutions for the δ-ALE-SPH model.

a snapshot of the absolute relative error $|\epsilon_{Vi}|$ at different spatial resolutions.

For $Re = 100$ (top panels), the sources of errors close to the top corners are rather clear even though they rapidly reduce as the resolution increases (from left to right). The relative errors reduce in space but not in intensity because of the singularities on the boundary conditions at the upper corners. For $Re = 1000$ (bottom panels) these reductions in space of $|\epsilon_{Vi}|$ are less evident and the errors levels are smaller with respect to the more viscous case. The global convergence analysis is depicted in Figure 15 where the time history of the global error ϵ_V is displayed. For both Reynolds numbers ϵ_V decreases as the spatial resolution increases even if the rate of convergence is larger for $Re = 100$. This figure also shows that the error on the global volume tends to increase during the simulation even though it maintains very small. The change on the convergence rates of ϵ_V deserve a more in-depth numerical analysis which is left for future works.

Finally, because of the conservation properties discussed in Section 4.1 and thanks to the mirroring of the field $(\boldsymbol{u} + \delta\boldsymbol{u}) \cdot \boldsymbol{n}$ on the ghost particles, the recorded global mass variations are at the machine precision for all the cases presented.

6.3 Dam-break flow impacting a vertical wall

This final benchmark is conceived to prove the reliability of the proposed scheme for free-surface problems. The initial configuration is described, for example, in [38] and reproduces the experimental campaign of [39].

In particular the fluid is initially confined in a reservoir on the left side of a rectangular tank and its right wall is suddenly removed to generate a fluid wedge as in Figure 16. The initial water heigh is H, the length of the reservoir is $B = 2H$

and the tank length is $L = 5.367H$.

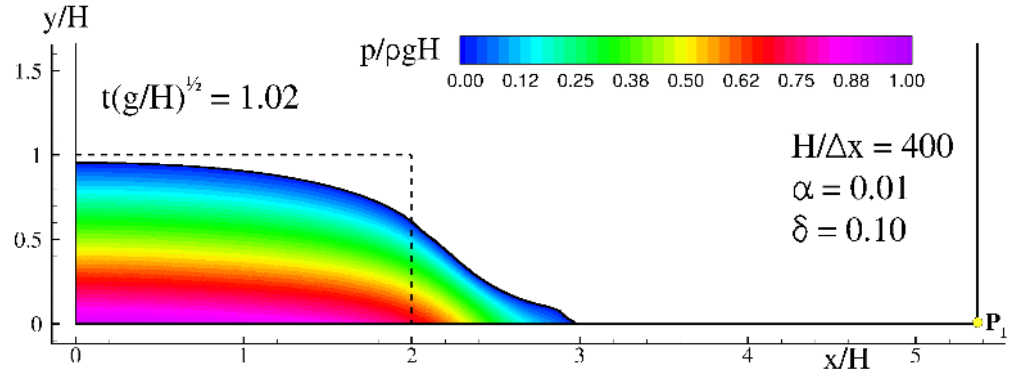

Fig. 16. Dam-break flow: early stages of the evolution of the pressure field as predicted by the δ-ALE-SPH model. Here α denotes the coefficient of the artificial viscosity while the symbol P_1 indicates the position of the pressure probe.

Both the standard SPH and the present δ-ALE-SPH are compared for this problem. In both the schemes the spatial resolution is $H/\Delta x = 400$ and the artificial viscosity is implemented (see, for example, [4]). Following [29] the shifting velocity of the δ-ALE-SPH model is modified to satisfy $\delta \boldsymbol{u} \cdot \boldsymbol{n} = 0$ close to the free-surface and preserve the free-surface kinematic boundary condition.

For what concerns the diffusive terms, this are switched off when the minimum eigenvalue of the Libersky renormalization matrix (15) is smaller than 0.2 (for more details see, for example, [29]). This avoids the use of diffusion in small jets and droplets where the renormalization matrices $\mathbb{L}_i$ may be ill-conditioned introducing numerical errors and instabilities with a possible reduction of the scheme robustness.

Figure 17 shows the instant of generation of the plunging wave and its reconnection with the underlying flow. Thanks to the action of the diffusive terms, the pressure field predicted by the δ-ALE-SPH model is much more regular than that obtained by using the standard SPH.

A substantial discrepancy between the Standard SPH and the δ-ALE-SPH schemes

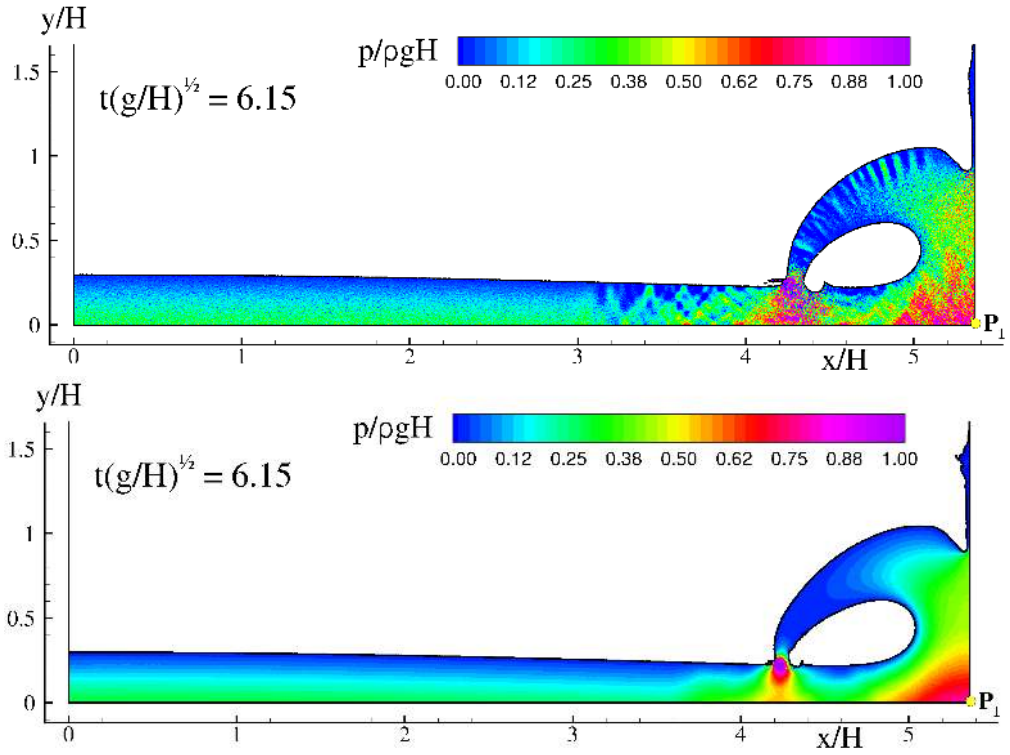

Fig. 17. Dam-break flow: pressure field as predicted by the standard SPH (top) and by the δ-ALE-SPH model (bottom). In both the models the spatial resolution is $H/\Delta x = 400$.

arises during the long-time evolution, that is when the fluid has already dissipated the largest part of its kinetic energy and is going to attain the final hydrostatic solution. In particular Figure 18 compares the pressure field as predicted by the standard SPH (top) and by the δ-ALE-SPH model (bottom) at $t\sqrt{g/H} = 30$. In the side panels the detailed views of the numerical solutions highlight that the pressure field of the standard SPH is affected by a sort of spot-like spurious noise.

This kind of disturbance is also observed for the volume variations (see the top panels of figure 19) and, more evidently, for the mass distribution (bottom panels of the same figure). In the latter case ϵ_{mi} is evaluated by using the mass of the particles that are initially along the free surface as reference value (namely, $m_0 = \rho_0 \, \Delta x^2$). Since the standard SPH the particles masses are advected Lagrangianly, their are transported without any time variation during the fluid evolution. Then, the field

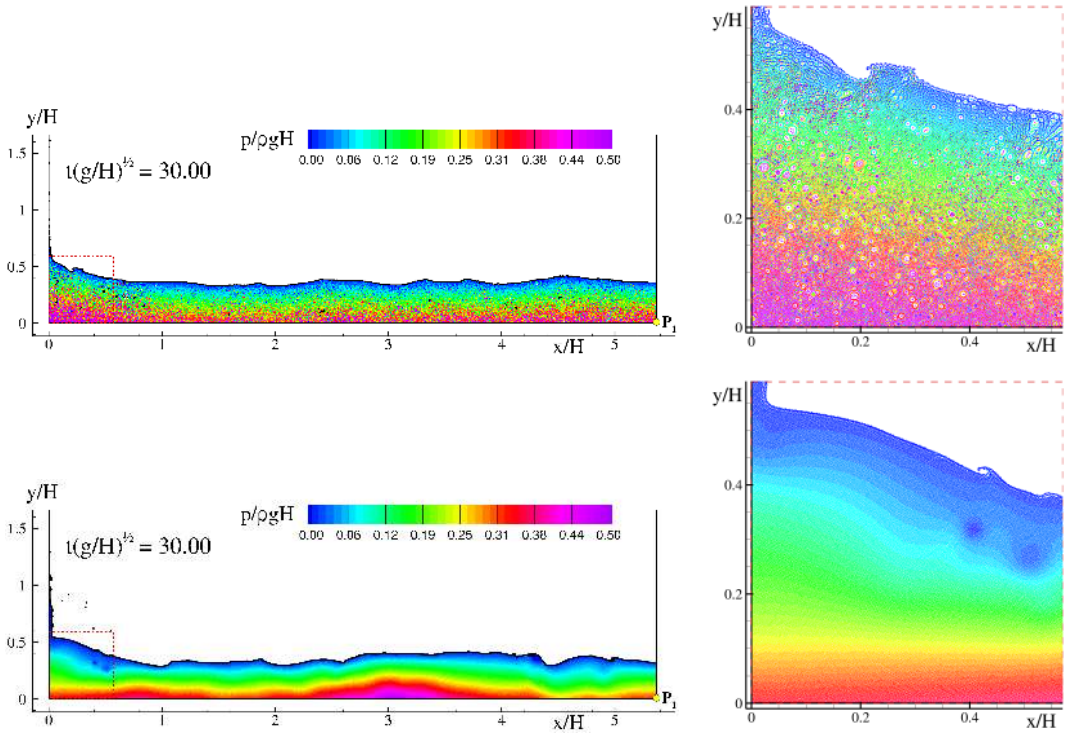

Fig. 18. Dam-break flow: long-time evolution of the pressure field as predicted by the standard SPH (top) and by the δ-ALE-SPH model (bottom). Side panels display a detail of the flow close to the left wall.

displayed in the bottom left panel of figure 19 is a consequence of the particle mixing occurred after several splash-up events. This noisy distributions on masses and volumes heavily affects the density and the pressure fields because of the algebraic relation $m = \rho V$ and the state equation $p = f(\rho)$. On the contrary, the proposed δ-ALE-SPH model, thanks to the diffusion on the particle masses and densities, is completely free from this spot-like disturbance as shown on the right column of figure 19.

7 Conclusion and Perspectives

In the present work we described a general way to obtain an Arbitrary-Lagrangian-Eulerian framework for the δ-SPH scheme with the Particle Shifting Technique.

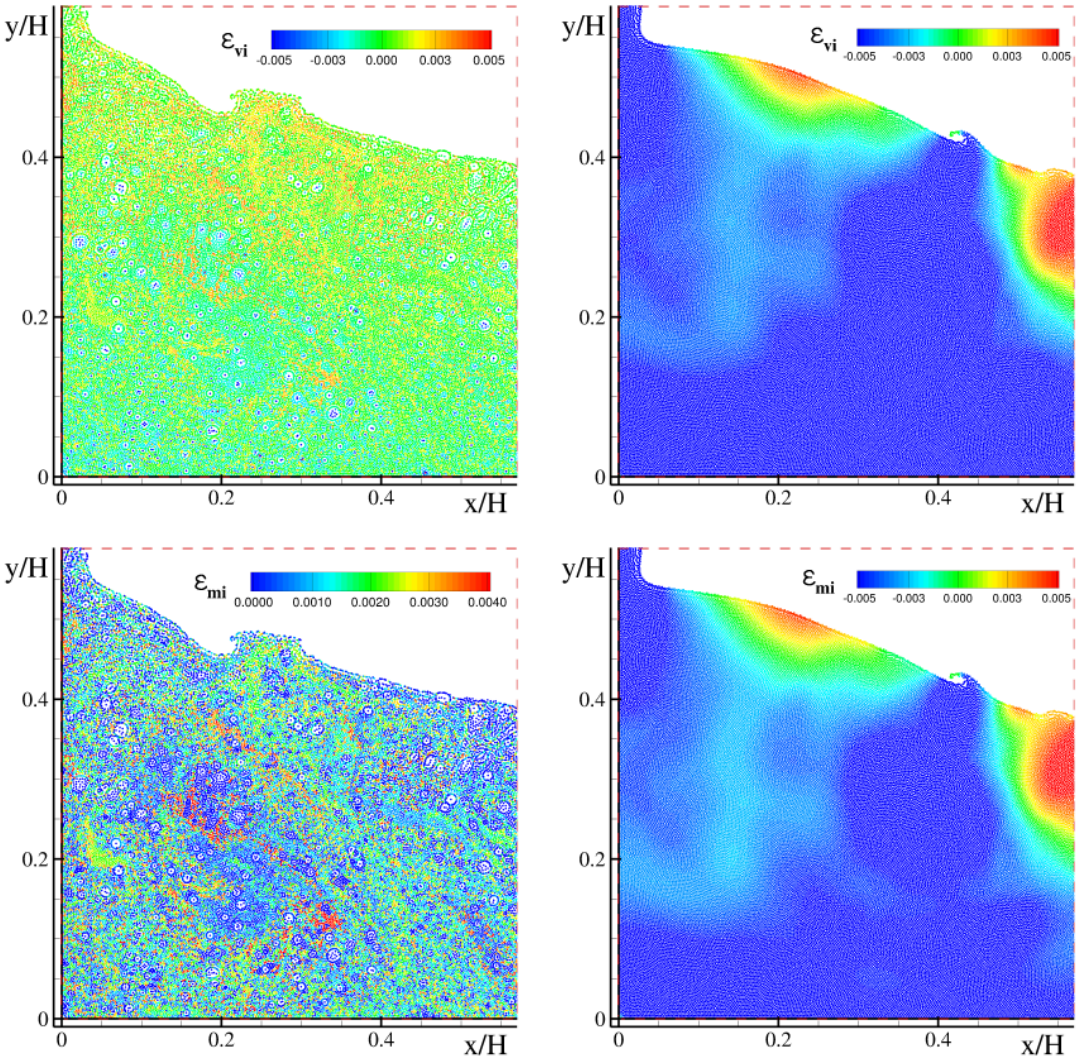

Fig. 19. Dam-break flow: details of the volume (top) and mass (bottom) variations close to the left wall at $t\sqrt{g/H} = 30$, as predicted by the standard SPH (left column) and the δ-ALE-SPH (right column).

The proposed model, named δ-ALE-SPH scheme, has been derived by rewriting the Navier-Stokes equations in the ALE formalism and, then, including the diffusive terms of the δ-SPH scheme in both the equations of density and mass. Finally, the arbitrary velocity field has been represented as the sum of the actual fluid velocity $\boldsymbol{u}$ and of a deviation field $\delta\boldsymbol{u}$, and the latter has been modelled through the Particle Shifting Technique described in Sun et al. [29]. It was shown that the above approach is, in fact, equivalent to the weak formulation proposed by Vila [33].

Three benchmark cases have been considered to test the δ-ALE-SPH scheme, namely the flow past an inclined elliptical cylinder with an angle of attack of 20° at $Re = 500$, the lid-driven cavity at $Re = 100$ and $Re = 1000$ and a dam-break flow. Two variants of the principal scheme have also been proposed, namely a scheme with constant volumes and a scheme with constant masses.

The first test case showed that the three models provide similar results in terms of forces, vorticity and pressure/density field while the mass and volume distributions display different behaviours because of their direct relation with the density field. Further, the use of the diffusive terms in the mass and density equations revealed of fundamental importance for the stability of the scheme. The second benchmark confirmed the robustness and accuracy of the δ-ALE-SPH scheme, providing a good agreement with the numerical solutions obtained through the models of Xu et al. [34] and Erturk et al. [14]. The presence of singularities at the cavity top corners was shown to influence the error on the total volume conservation though the latter remains limited. Conversely, the mass conservation for this confined test case was preserved by the δ-ALE-SPH scheme. Finally, the dam-break flow proved the reliability of the proposed scheme in simulating free-surface problems and its ability in overcoming some of the drawback of the standard Lagrangian SPH model.

The overall investigation highlighted that the ALE-SPH schemes, whose differential operators are usually represented by using Riemann solvers (Vila [33]), can be alternatively implemented by adding suitable diffusive terms. This latter approach leads to the definition of an ALE-SPH schemes with properties of stability and accuracy comparable to the Riemann-based models.

Remarkably, the variant of the δ-ALE-SPH with constant masses coincides with the δ^+-SPH scheme described in Sun et al. [29], bridging the gap between the

weak formulation of Vila [33] and the standard approach from Lagrangian Navier-Stokes equations. In fact, the numerical simulations showed that the general δ-ALE-SPH and the δ^+-SPH scheme are practically equivalent in terms of accuracy and conservation properties.

Acknowledgements

The research activity has been developed within the Project Area Applied Mathematics of the Department of Engineering, ICT and Technology for Energy and Transport (DIITET) of the Italian National Research Council (CNR).

The work also received funds by the National Project of Numerical Wind Tunnel of China (Grant No. 2018-ZT2B05). The author PengNan Sun has been funded by a post-doctoral research grant from the Ecole Centrale de Nantes.

References

[1] M. Antuono and A. Colagrossi. The damping of viscous gravity waves. *Wave Motion*, 50(0):197–209, 2012.

[2] M. Antuono, A. Colagrossi, S. Marrone, and D. Molteni. Free-surface flows solved by means of SPH schemes with numerical diffusive terms. *Computer Physics Communications*, 181(3):532–549, 2010.

[3] M. Antuono, A. Colagrossi, S. Marrone, and C. Lugni. Propagation of gravity waves through an SPH scheme with numerical diffusive terms. *Computer Physics Communications*, 182(4):866–877, 2011.

[4] M. Antuono, A. Colagrossi, and S. Marrone. Numerical diffusive terms in

weakly-compressible SPH schemes. *Computer Physics Communications*, 183 (12):2570–2580, 2012.

[5] M. Antuono, B. Bouscasse, A. Colagrossi, and S. Marrone. A measure of spatial disorder in particle methods. *Computer Physics Communications*, 185 (10):2609–2621, 2014.

[6] M. Antuono, S. Marrone, A. Colagrossi, and B. Bouscasse. Energy balance in the δ-SPH scheme. *Computer Methods in Applied Mechanics and Engineering*, 289:209–226, 2015.

[7] B. Bouscasse, A. Colagrossi, S. Marrone, and M. Antuono. Nonlinear water wave interaction with floating bodies in SPH. *Journal of Fluids and Structures*, 42:112–129, 2013.

[8] A. Colagrossi and M. Landrini. Numerical Simulation of Interfacial Flows by Smoothed Particle Hydrodynamics. *Journal of Computational Physics*, 191: 448–475, 2003.

[9] A. Colagrossi, M. Antuono, and D. Le Touzé. Theoretical considerations on the free-surface role in the Smoothed-particle-hydrodynamics model. *Physical Review E*, 79(5):056701, 2009.

[10] A. Colagrossi, M. Antuono, A. Souto-Iglesias, and D. Le Touzé. Theoretical analysis and numerical verification of the consistency of viscous smoothed-particle-hydrodynamics formulations in simulating free-surface flows. *Physical Review E*, 84:026705, 2011.

[11] A. Colagrossi, B. Bouscasse, M. Antuono, and S. Marrone. Particle packing algorithm for SPH schemes. *Computer Physics Communications*, 183(2):1641–1683, 2012.

[12] A. Colagrossi, E. Rossi, and M. Marrone. The Discrete Vortex Hydrodynamics method:analogies and differences with the SPH method. *Communications in Computational Physics*, 20:660–688, 2016.

[13] M. De Leffe, D. Le Touzé, and B. Alessandrini. A modified no-slip condition in weakly-compressible SPH. In *6th ERCOFTAC SPHERIC workshop on SPH applications*, pages 291–297, 2011.

[14] Ercan Erturk, Thomas C Corke, and Cihan Gökçöl. Numerical solutions of 2-d steady incompressible driven cavity flow at high reynolds numbers. *International journal for Numerical Methods in fluids*, 48(7):747–774, 2005.

[15] N. Grenier, D. Le Touzé, A. Colagrossi, M. Antuono, and G. Colicchio. Viscous bubbly flows simulation with an interface SPH model. *Ocean Engineering*, 69: 88–102, 2013.

[16] A. Khayyer, H. Gotoh, and Y. Shimizu. Comparative study on accuracy and conservation properties of two particle regularization schemes and proposal of an optimized particle shifting scheme in ISPH context. *Journal of Computational Physics*, 332:236–256, 2017.

[17] PK Kundu and LM Cohen. Fluid mechanics, 638 pp. *Academic, Calif*, 1990.

[18] D. Le Touzé, A. Colagrossi, G. Colicchio, M. Greco. A critical investigation of smoothed particle hydrodynamics applied to problems with free-surfaces. *Int. J. Numer. Meth. Fluids* 73: 660–691, 2013

[19] S.J. Lind, R. Xu, P.K. Stansby, and B.D. Rogers. Incompressible smoothed particle hydrodynamics for free-surface flows: A generalised diffusion-based algorithm for stability and validations for impulsive flows and propagating waves. *Journal of Computational Physics*, 231(4):1499–1523, 2012.

[20] R. Nestor, M. Basa, M. Lastiwka, N.J. Quinlan. Extension of the finite volume particle method to viscous flow. *Journal of Computational Physics*,228(5): 1733–1749, 2009.

[21] S. Marrone, M. Antuono, A. Colagrossi, G. Colicchio, D. Le Touzé, and G. Graziani. Delta-SPH model for simulating violent impact flows. *Computer Methods in Applied Mechanics and Engineering*, 200(13-16):1526–1542, 2011.

[22] S. Marrone, A. Colagrossi, M. Antuono, G. Colicchio, and G. Graziani. An accurate SPH modeling of viscous flows around bodies at low and moderate Reynolds numbers. *Journal of Computational Physics*, 245:456–475, 2013.

[23] S. Marrone, A. Colagrossi, A. Di Mascio, and D. Le Touzé. Prediction of energy losses in water impacts using incompressible and weakly compressible models. *Journal of Fluids and Structures*, 54:802–822, 2015.

[24] G. Oger, S. Marrone, D. Le Touzé, and M. de Leffe. SPH accuracy improvement through the combination of a quasi-Lagrangian shifting transport velocity and consistent ALE formalisms. *Journal of Computational Physics*, 313:76–98, 2016.

[25] N.J. Quinlan, M. Lastiwka, and M. Basa. Truncation error in mesh-free particle methods. *International Journal for Numerical Methods in Engineering*, 66(13): 2064–2085, 2006.

[26] E. Rossi, A. Colagrossi, B. Bouscasse, and G. Graziani. The Diffused Vortex Hydrodynamics method. *Communications in Computational Physics*, 18(2): 351–379, 2015.

[27] P. N. Sun, A. Colagrossi, S. Marrone, and A. M. Zhang. Detection of Lagrangian Coherent Structures in the SPH framework. *Computer Methods in Applied Mechanics and Engineering*, 305:849–868, 2016.

[28] P. N. Sun, A. Colagrossi, S. Marrone, and A. M. Zhang. The δplus-SPH model: Simple procedures for a further improvement of the SPH scheme. *Computer Methods in Applied Mechanics and Engineering*, 315:25–49, 2017.

[29] P. N. Sun, A. Colagrossi, S. Marrone, M. Antuono, and A. M. Zhang. A consistent approach to particle shifting in the δ-Plus-SPH model. *Computer Methods in Applied Mechanics and Engineering*, 348:912–934, 2019.

[30] Peng-Nan Sun, Andrea Colagrossi, and A-Man Zhang. Numerical simulation of the self-propulsive motion of a fishlike swimming foil using the δ^+-SPH model.

Theoretical and Applied Mechanics Letters, 8(2):115–125, 2018.

[31] P.N. Sun, A. Colagrossi, S. Marrone, M. Antuono, and A.M. Zhang. Multi-resolution Delta-plus-SPH with tensile instability control: Towards high Reynolds number flows. *Computer Physics Communications*, 224:63–80, 2018.

[32] J.J. Monaghan SPH without a tensile instability. *J. Comput. Phys.* 159: 290–311, 2000

[33] J.P. Vila. On particle weighted methods and Smooth Particle Hydrodynamics. *Mathematical Models & Methods in Applied Sciences*, 9(2):161–209, 1999.

[34] R. Xu, P. Stansby, and D. Laurence. Accuracy and stability in incompressible SPH (ISPH) based on the projection method and a new approach. *Journal of Computational Physics*, 228(18):6703–6725, 2009.

[35] A-Man Zhang, Peng-Nan Sun, Fu-Ren Ming, and A Colagrossi. Smoothed particle hydrodynamics and its applications in fluid-structure interactions. *Journal of Hydrodynamics, Ser. B*, 29(2):187–216, 2017.

[36] M. D. Green, R. Vacondio, and J. Peiró. A smoothed particle hydrodynamics numerical scheme with a consistent diffusion term for the continuity equation. *Computers & Fluids*, 179: 632–644, 2019.

[37] D.D. Meringolo, F. Aristodemo, and P. Veltri. SPH numerical modeling of waveperforated breakwater interaction. *Coastal Engineering*, 101: 48–68, 2015.

[38] S. Marrone, A. Colagrossi, A. Di Mascio, D. Le Touzé, Analysis of free-surface flows through energy considerations: Single-phase versus two-phase modeling. *Physical Review E*, 93, 053113, 2016

[39] L. Lobovsky, E. Botia-Vera, F. Castellana, J. Mas-Soler, A. Souto-Iglesias, Experimental investigation of dynamic pressure loads during dam break *Journal of Fluids and Structures*, 48: 407–434, 2014